




# A Critical Review of the Use of Graphene-Based Gas Sensors

Aniket Chakraborty<sup>1,2</sup>, Suresh Nuthalapati<sup>1,2</sup>, Anindya Nag<sup>1,2,\*</sup>, Nasrin Afsarimanesh<sup>3</sup>,  
Md. Eshrat E Alahi<sup>4</sup> and Mehmet Ercan Altinsoy<sup>1,2</sup>

<sup>1</sup> Faculty of Electrical and Computer Engineering, Technische Universität Dresden, 01062 Dresden, Germany

<sup>2</sup> Centre for Tactile Internet with Human-in-the-Loop (CeTI), Technische Universität Dresden, 01069 Dresden, Germany

<sup>3</sup> School of Civil and Mechanical Engineering, Curtin University, Perth, WA 6102, Australia

<sup>4</sup> Institute of Biomedical and Health Engineering, Shenzhen Institutes of Advanced Technology, Chinese Academy of Sciences, Shenzhen 518055, China

\* Correspondence: anindya1991@gmail.com

**Abstract:** The employment of graphene for multifunctional uses has been a cornerstone in sensing technology. Due to its excellent electrochemical properties, graphene has been used in its pure and composite forms to detect target molecules over a wide range of surfaces. The adsorption process on the graphene-based sensors has been studied in terms of the change in resistance and capacitance values for various industrial and environmental applications. This paper highlights the performance of graphene-based sensors for detecting different kinds of domestic and industrial gases. These graphene-based gas sensors have achieved enhanced output in terms of sensitivity and working range due to specific experimental parameters, such as elevated temperature, presence of particular gas-specific layers and integration with specific nanomaterials that assist with the adsorption of gases. The presented research work has been classified based on the physical nature of graphene used in conjugation with other processed materials. The detection of five different types of gases, including carbon dioxide (CO<sub>2</sub>), ammonia (NH<sub>3</sub>), hydrogen sulphide (H<sub>2</sub>S), nitrogen dioxide (NO<sub>2</sub>) and ethanol (C<sub>2</sub>H<sub>5</sub>OH) has been shown in the paper. The challenges of the current graphene-based gas sensors and their possible remedies have also been showcased in the paper.

**Keywords:** graphene; sensors; gas; reduced graphene oxide; graphene quantum dots



**Citation:** Chakraborty, A.; Nuthalapati, S.; Nag, A.; Afsarimanesh, N.; Alahi, M.E.E.; Altinsoy, M.E. A Critical Review of the Use of Graphene-Based Gas Sensors. *Chemosensors* **2022**, *10*, 355. <https://doi.org/10.3390/chemosensors10090355>

Academic Editor: Ali Othman

Received: 1 August 2022

Accepted: 29 August 2022

Published: 1 September 2022

**Publisher's Note:** MDPI stays neutral with regard to jurisdictional claims in published maps and institutional affiliations.



**Copyright:** © 2022 by the authors. Licensee MDPI, Basel, Switzerland. This article is an open access article distributed under the terms and conditions of the Creative Commons Attribution (CC BY) license (<https://creativecommons.org/licenses/by/4.0/>).

## 1. Introduction

In the current era of nanotechnology, graphene has been one of the most significant discoveries [1,2] in the microelectronics world. The range of prototypes that can be developed using graphene has fascinated researchers over the years. The work shown by Giem et al. [3] showed the rise in this carbon-based material with unusual and exceptional electron mobility properties. Although graphite is available in nature and has been used for sensing applications [4–6], the ability to transform graphite into graphene widened its application spectrum due to its fabrication in the laboratories, easy customization and exceptional mechanical strength [7–10]. This led the researchers to use graphene for fabricating prototypes that played a crucial role in electrochemical [11–13] and strain-sensing [14–17] applications. Some of the advantages of these graphene-based sensors have been their easy operating principle, high robustness, excellent durability and efficient performance in terms of sensitivity and longevity [16,18]. Being a carbon allotrope, it has been used to form biocompatible sensors that have been used for wearable sensing applications [19,20]. Although other carbon allotropes such as carbon nanotubes (CNTs) [21–23] and graphite [24–26] have been considered for sensing applications, the unique electrical, mechanical and thermal characteristics of graphene have made it a much more superior material as compared to its counterparts. It has been able to integrate with both rigid and flexible substrates for sensing purposes. Some of the common materials with which graphene has formed

pure and composite electrodes are silicon [27,28], polydimethylsiloxane (PDMS) [29,30], polyethylene terephthalate (PET) [31,32], polyimide (PI) [33,34], polyaniline [35,36] and poly(3,4-ethylenedioxythiophene) polystyrene sulfonate (PEDOT: PSS) [37,38]. Another big attribute of graphene is its ability to easily conjugate with other nanomaterials and polymers, which has helped it form sensors with high selectivity and specificity [39,40]. The high electrical conductivity and mechanical flexibility of graphene have allowed it to be used for electrochemical [41,42] and strain [43–46] sensing applications. This paper explains the use of graphene sensors, particularly for gas sensing applications. The electrochemical nature of the prototypes has been tested via introspecting the change in their responses due to the presence of gases in controlled environments. The classification is based on four types of graphene nanostructures, namely graphene nanosheets [47,48], graphene quantum dots (GQDs) [49,50], graphene nanoplatelets (GNPs) [51,52], and reduced graphene oxide (rGO) [53,54] which has been conducted to analyze the differences in their sensing performances in terms of sensitivity and operating range. These single-layered and multi-layered graphene allotropes have been fabricated using different approaches, such as mechanical exfoliation [55,56], epitaxial growth [57,58], chemical vapour deposition (CVD) [59,60], laser ablation [61,62] and chemical reduction [63,64]. While all these methodologies have their respective advantages, the laser ablation or pulsed layer deposition (PLD) technique is the most popular due to certain advantages, such as simple fabrication process, low growth temperature, easy customization, low cost and high-cost control of thickness and morphology [65]. The graphene types have formed highly efficient sensing prototypes in terms of sensitivity, robustness and longevity. While using the graphene-based sensors for electrochemical sensing applications, the detection of the target analyte is conducted with high specificity due to the high electron mobility and electrical conductivity of the graphene layers. The graphene allotropes have been used as pure or composites forms to develop the chemo resistive gas sensors.

The different allotropic forms of graphene used for gas-sensing purposes are chosen on the basis of specific parameters of their physical structures, e.g., hybridization and bond length. For example, as compared to graphene, GQDs exhibit different behavior such as non-zero bandgap, making them a 2D graphene material. The average value of the angles between C-H and C-H bonds, as the suggestion by [66], is smaller than the tetrahedral angle of  $109.5^\circ$ , suggesting the nature of these bonds is  $sp^3$ -like. It also has special edge and quantum confinement effects, as opposed to other carbon-based materials such as carbon dots, CNTs and fullerenes [67]. Figure 1 [68] shows the electronic and optical properties of graphene. Comparatively, the graphene nanosheets are the thinnest material, with a thickness of 0.34 nm. These nanosheets consist of a single layer of carbon atoms having hexagonal lattices. The rGO has been used widely due to its high surface area with a similar carbon-to-carbon bond length of 0.142 nm for graphene and 0.127 nm for graphite. With the adsorption of hydrogen ions, one of the structural changes that can be seen in graphene is the change in lattice constant of graphene changes from 0.245 nm to 0.25 nm with the buckling effect. This leads to a subsequent change in structural variation and electronic properties of graphene. Studying the chiral structures of graphene, when every carbon atom is bounded to adjacent three carbon atoms and a hydrogen atom, the structure is found to be non-magnetic and semiconducting with a direct local density approximation band gap of 3.9 eV. When pristine graphene is reacted with the gaseous molecules, there is no change in the band structure at the vicinity of the Fermi level. Apart from an additional gas-sensitive layer, the doping of the graphene electrodes changes the Fermi level according to the chosen ion [69].

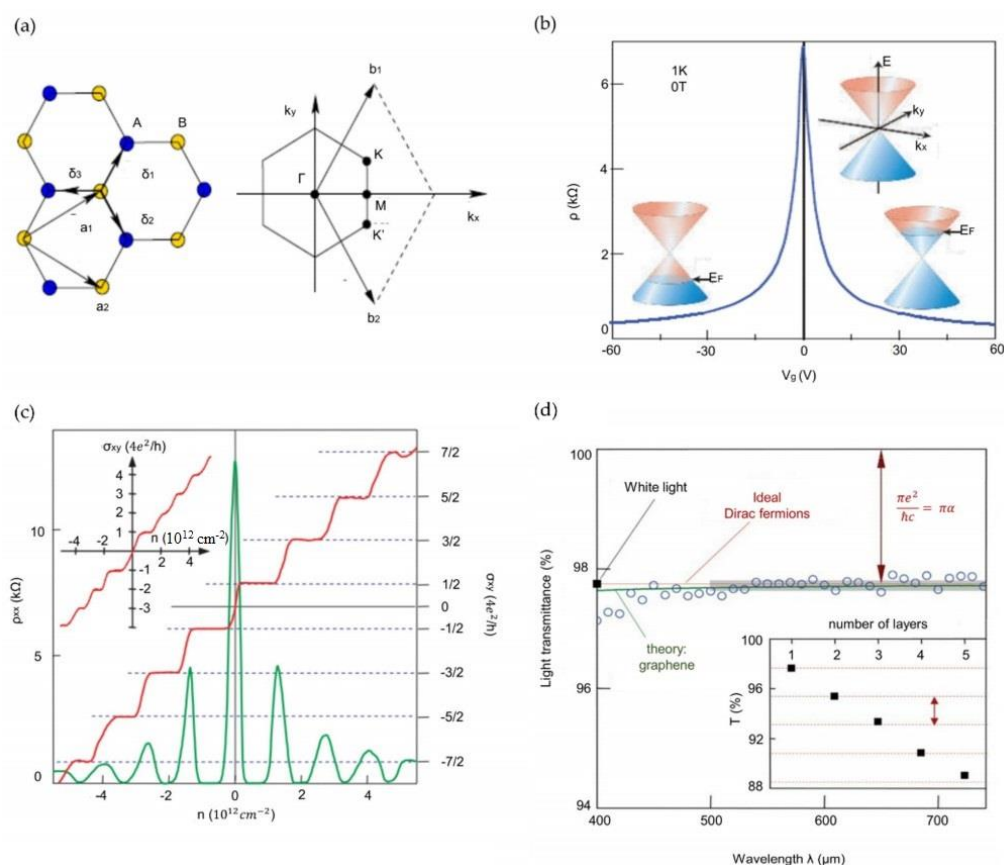


**Figure 1.** Electronic and optical properties of graphene. (a) Hexagonal lattice structure (left) and its Brillouin zone (right). (b) Ambipolar electric effect of single-layer graphene. (c) Response of graphene in terms of hall conductivity (red) and longitudinal resistivity (green) with respect to the carrier concentration. (d) Transmittance spectrum of single-layered graphene. Reproduced from Sang, M., Shin, J., Kim, K., and Yu, K.J., 2019. Electronic and thermal properties of graphene and recent advances in graphene-based electronics applications. *Nanomaterials*, 9(3), p. 374 [68].

The performance of these graphene-based sensors has been highly dependent on their fabrication processes. For example, the graphene generated using the CVD process has certain advantages, such as being high quality, having high homogeneity, and having excellent control over the number of layers. Given these benefits, the synthesized graphene would be highly porous, which would be an advantage for electrochemical applications. Among the various categories of CVD, plasma-enhanced CVD (PECVD) is more advantageous in comparison to other ones as the growth is more efficient due to the presence of highly active free radicals [70]. The synthesis process could also be carried out on dielectric or insulating substrates, thus performing the operation at lower temperatures. This allows the samples to be used for semiconducting applications. A lot of researchers have preferred this fabrication technique due to the formation of graphene with a large specific surface area and high carrier mobility. This allows the formation of prototypes with small size, low power, low cost, and high sensitivity. These sensors are also able to perform with a low energy barrier for the adsorption of gas molecules. Other techniques e.g., mechanical exfoliation also achieve graphene with high quality and purity, but the obtained flakes are poor for industrial purposes. The work on gas sensors [71–76] has been very significant in recent times due to the permanent changes they cause to the environment. The change in the concentration of the gases, even in minute values, can create permanent damage to the health of human beings and the environment. Some of the disastrous effects that can be caused due to the abruptness in the equilibrium of the gases are extreme weather, food supply disruptions and increased climatic changes [77,78]. Even in industrial and

domestic scenarios, the presence of dangerous gases in minuscule concentrations can lead to injurious and death. Thus, it has always been state-of-the-art to develop highly efficient gas sensors. Even though topic reviews on gas sensors have been written earlier, none of the papers have provided a substantial review on these gas sensors or have provided an integrated view of the detection of different kinds of gases based on the physiochemical forms of graphene. The performances of the sensors are shown for five types of gases, namely carbon dioxide (CO<sub>2</sub>) [79,80], ammonia (NH<sub>3</sub>) [81,82], hydrogen sulphide (H<sub>2</sub>S) [83,84], nitrogen dioxide (NO<sub>2</sub>) [85,86] and ethanol (C<sub>2</sub>H<sub>5</sub>OH) [54,87]. Although the quality of these sensors has been depicted for a combination of these mentioned gases, the whole spectrum has not been provided yet. The novelty of this paper lies in two aspects. Firstly, the classification of the type of graphene allotrope used for developing the gas sensors has not been conducted yet. Secondly, the detection of five primary gases pivotal for industrial applications, as shown in this paper, has not been shown yet. The quantitative efficiency of the dynamic characteristics of the graphene-based sensors has been showcased to subsequently represent their qualitative capabilities. The examples are shown in this paper differentiating the type of prototypes based on the nature of graphene subsequently calls attention to their performances as well. The rest of the manuscript is organized as follows. Followed by section one highlighting the significance of graphene and gas sensors, the working mechanism of these graphene-based gas sensors is explained in section two. Section three elucidates some of the significant examples related to these sensors, where a categorization has been provided based on the four types of graphene. As these four types differ in terms of their physiochemical nature, the sensors shown in each of these types have been able to detect different kinds of gases. This is followed by showcasing some of the challenges existing with the current sensors and their possible remedies. The conclusion is drawn in the final section of the paper.

## 2. The Working Mechanism of the Sensors

The operating principle of the graphene-based gas sensors is based on the change in the electrical responses with respect to the presence of the gaseous molecules. When the prototype senses the gases in the atmosphere, a corresponding potential difference is obtained based on the concentration of the gas. This difference is measured in terms of current or resistance values. The nature of the detected gases depends on the sensing element present in the sensing area of the prototypes. There are different types of gas sensors available based on the type of sensing element. Some of the common ones include metal oxide [88], optical [89], electrochemical [90], capacitance [91], calorimetric [92] and acoustic [93] gas sensors. Each of these sensing types includes different kinds of gas sensor testing equipment to measure the gas sensor characteristics of each sensor. The most common ones include the chemiresistive sensors, which consist of a sensing element that consists of free donor electrons. The chemiresistive graphene-based gas sensors normally use the surface-dominated adsorption process as the mechanism during the detection process. The change in the electrical signal is measured in terms of resistance due to the adsorption of the gas analytes onto the sensitive material [94]. When the target gas with different concentrations of gas is exposed to the sensor, the ability of the graphene sensors to detect them is tested via the change in the relative resistance. The resistance value when the sensor is in the air, and that in the target gases is used to define the sensitivity of the sensors. The sensitivity for oxidizing gases and reducing gases are defined below:

$$S_g = (|R_g - R_a| / R_a) \times 100 \quad \text{Oxidizing gas} \quad (1)$$

$$S_g = (|R_a - R_g| / R_a) \times 100 \quad \text{Reducing gas} \quad (2)$$

where  $R_a$  is the sensor resistance in air and  $R_g$  is the sensor resistance in target gas.

The conductivity of the gas-sensitive layer varies with respect to certain factors, such as surface morphology and thickness, which in turn depends on the preparation method. The insulative substrate interface is another factor that contributes to the change in the

conductivity of the prototypes. Thus, the variation in the degree of hydration caused due to the interference of water vapors while experimenting at room temperature subsequently changes the overall response. This way, a lot of experiments are carried out at elevated temperatures in a laboratory environment. In the case of real-time situations, the presence of internal heaters assists in maintaining high temperatures and reducing the hydration effect. The concentrations of each target gas are generally adjusted by controlling the flow ratio between balance gas (air) and calibration gas, which is achieved by using mass-flow controllers (MFC). The sensor response generally increases as the concentration of the gas increases. In an n-type semiconductor, resistance decreases with time as gas concentration (a reducing gas) increases and increases as gas concentration decreases (oxidizing gas). The response time ( $R_{res}$ ) and recovery time ( $R_{rec}$ ) of the sensors are defined to be the duration taken by the prototypes to reach their maximum sensitivity and come back to their original state, respectively.

### 3. Graphene-Based Gas Sensors

The following sub-sections highlight the work performed by different researchers on the detection of a wide range of gases. The graphene allotropes have been used in the sensing area of the prototypes to detect the presence of gases at varying concentrations. The prototypes have been responsible for detecting single or multiple gases when used as per their application. Along with graphene, other conductive and semiconducting nanomaterials have also been integrated into the prototypes to increase their specificity and selectivity. The covalent bonding between the gaseous molecules and graphene-assisted sensors leads to a significant change in the chemical response of the sensors.

#### 3.1. Graphene Nanosheets-Based Gas Sensors

Graphene nanosheets [95,96] are the most commonly used graphene allotropes to be used for multifunctional sensing applications. Some of the advantages include a high electrical conductivity, lightweight and mechanical flexibility, which make them a popular choice for use in gaseous applications [97,98]. The porous nature of graphene nanosheets increases the probability of the adsorption of different gas molecules on the sensing area of the prototypes. The exchange in electrons takes place when the gases act as donors or acceptors, thus altering the resistive values of the sensors.

##### (1) Carbon-dioxide sensors

H.J. Yoon et al. [99] described a graphene-based CO<sub>2</sub> gas sensor made via mechanical cleavage and micromachining. Graphene was stamped onto a silicon substrate using PDMS. When exposed to varying atmospheric CO<sub>2</sub> concentrations, the graphene sensor exhibits considerable conductance changes. On the graphene sheet, the CO<sub>2</sub> gas molecule functions as both a donor and an acceptor. A charge transfer between both the graphene sheet and CO<sub>2</sub> gas is shown by a change in graphene conductance. The CO<sub>2</sub> gas sensor response time is 8 s. The recovery period lasts, on average, 10 s. The ratio of conductance change rose from 9 to 26% when the CO<sub>2</sub> concentration increased from 10 to 100 ppm at 22 °C at 44% humidity. For the measurement range, the sensor's estimated CO<sub>2</sub> sensitivity was 0.17%/ppm. It suggested that CO<sub>2</sub> molecules are more easily adsorbed or desorbed on graphene than other types of gas molecules.

##### (2) Nitrogen oxide sensors

Zhu et al. [100] describe a hydrothermally produced porous composite film that uses rGO nanosheets as the base material for copper (Cu<sub>2</sub>O) nanowires and nanoparticles. The investigation into the sensor's performance was focused on the sensing response, selectivity, optimum working temperature, long-term stability, repeatability, and humidity impact on the sensing of NO<sub>2</sub> gas. As one of the best cases of Cu<sub>2</sub>O-related NO<sub>2</sub> detection regarding sensor response and operating temperature, the sensor response reached 0.66 to 50 ppb NO<sub>2</sub> gas with complete recovery at room temperature. With increased carrier gas temperature, the device's responses decreased. As a result of the most responses, we found that room

temperature was the optimum one. The response and recovery times when it was exposed to NO<sub>2</sub> gas to 50 ppm were found as 279 s and 1239 s, respectively. In comparison to other interference gases, a higher selectivity towards NO<sub>2</sub> gas was observed. Chen et al. [101] offer a quick and efficient method utilizing lyophilization to turn 2D plane graphene-based nanosheets into 3D crumpled structures based on non-covalent bonding changes. Figure 2a,b [101] shows the schematic diagram of the fabrication process of these sensors. When compared to other graphene-based materials, the 3D-crumpled NA-rGO nanosheets (CNN) sensors showed the highest response, with a value of 3.8 toward 10 ppm NO<sub>2</sub> gas. The 3D-CNN sensors also showed excellent NO<sub>2</sub> gas selectivity. As predicted, the response increased gradually as NO<sub>2</sub> concentration increased, and the response and recovery time were consistent at all concentrations. Additionally, the multiple response and recovery curve for the 3D-CNN sensors showed excellent stability and reliability. The response and recovery time towards 10 ppm NO<sub>2</sub> gas were maintained at 8 s and 53 min, respectively.

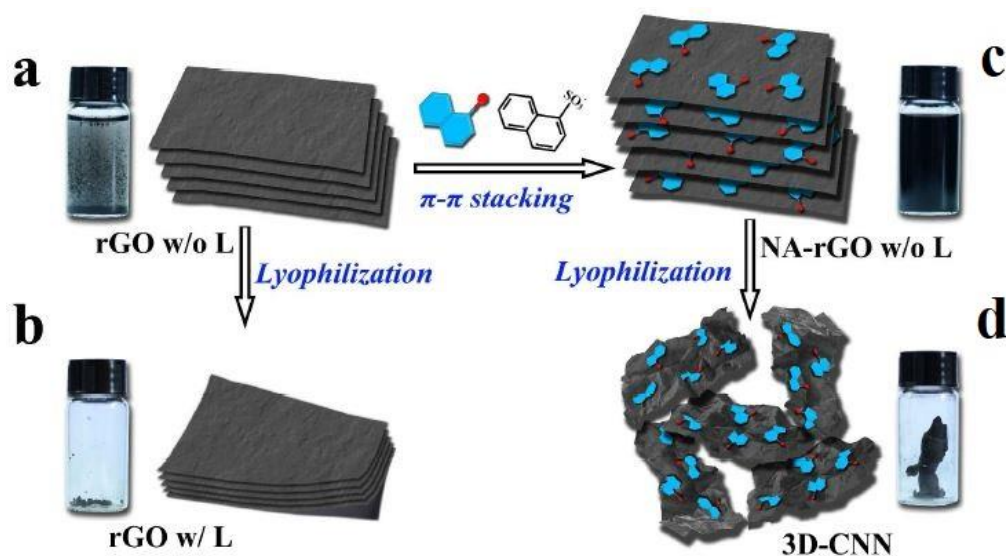


**Figure 2.** Schematic diagram of the fabrication process of 3D-crumpled NA-rGO nanosheets for NO<sub>2</sub> gas detection. (a,b) The formation of aggregated 2D plane rGO nanosheets with the lyophilization process. (c) Dispersion of 2D plane NA-rGO nanosheets with the lyophilization process. (d) The lamination and separation of 3D crumpled NA-rGO nanosheets with the lyophilization process [101]. Reproduced from Chen, Z., Wang, J., Umar, A., Wang, Y., Li, H. and Zhou, G., 2017. Three-dimensional crumpled graphene-based nanosheets with ultrahigh NO<sub>2</sub> gas sensibility. *ACS applied materials & interfaces*, 9(13), pp. 11819–11827.

Srivastava et al. [102] employed B- and N-codoped graphene nanosheets that were successfully developed on a Cu foil substrate using the LPCVD process, and they were then deposited onto Si/SiO<sub>2</sub> for extremely high NO<sub>2</sub> sensing at room temperature. Then, using pre-patterned gold (Au) electrodes, the produced nanosheets were transferred to Si/SiO<sub>2</sub> substrates. Using a spin coater and air drying, a thin layer of PMMA was applied to the top layer of the graphene films during the transfer process. By exposing the sensor to NO<sub>2</sub> gas and monitoring the related resistance change over time, the gas sensing abilities of Gr- and BNGr-based sensors were tested. The BNGr sensor had a response of 0.05% for 1 ppb NO<sub>2</sub> and 3.29% for 5 ppm NO<sub>2</sub> gas as the NO<sub>2</sub> gas concentration increases from 1 to 80 ppb, the BNGr sensor's sensor response increases. For the initial cycle, the sensors recovered very quickly, while the sensor took longer to fully recover as time passed on and concentration levels increased. Figure 3 [102] shows the schematic diagram of the distribution of charge densities on the surface of pure graphene and BN-doped graphene electrodes for the NO<sub>2</sub> molecules. For 1 ppb NO<sub>2</sub> gas, the BNGr sensor's response time and recovery time were also calculated and found to be 177 s and 392 s, respectively. Comparing the BNGr sensor to the Gr sensor, the BNGr sensor exhibits a higher response and faster detection. It was

observed that when compared to other gaseous species,  $\text{NO}_2$  gas had a considerably higher response from the BNGr sensor. Shaik et al. [103] used GO hydrothermal method, treated with ammonia solution to produce nitrogen-doped graphene nanosheets. This method allows for the simultaneous reduction of graphene oxide and doping of nanosheets with nitrogen atoms. The drop-drying method was used to synthesize thin films of graphene sheets, and nitrogen-doped graphene sheets on pre-patterned gold interdigitated electrodes (IDEs). The NGS's sensing abilities at different  $\text{NO}_2$  gas concentrations at room temperature were examined. Both sensors' conductivity increases when the target gas is turned on and recovers after being cleared with nitrogen flow. Even in a flow of nitrogen gas, the signal requires 90 to 120 min to recover in the absence of UV light irradiation. But when illuminated with UV light, the recovery time was shortened to 15 min. From the test, it was found that as the concentration of the gas increases, the responses also increase gradually. The average decrease in sensor response after six consecutive cycles is approximately 14% of the initial response. It was noticed that the sensor response declines gradually as the number of response-recovery cycles increases. This proved the good reproducibility of the NGS/IDE sensor.

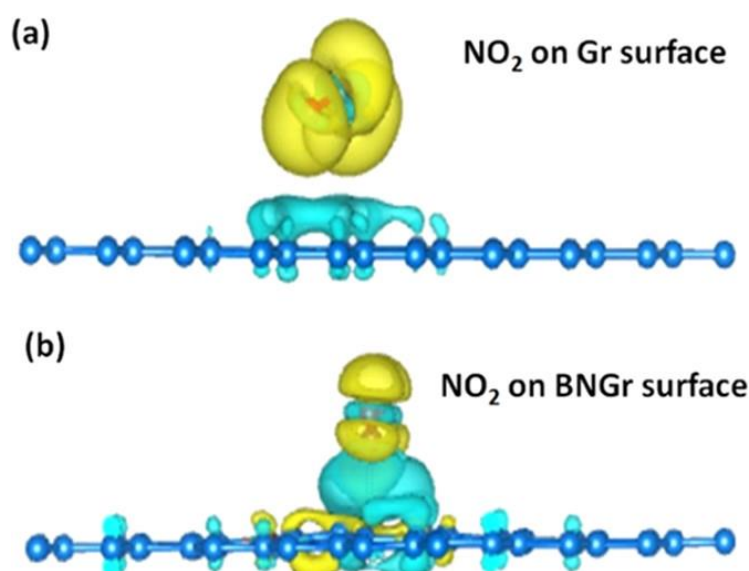


**Figure 3.** Charge densities of the (a) graphene and (b) BN-graphene surface with  $\text{NO}_2$  molecules [102]. Reproduced from Srivastava, S., Pal, P., Sharma, D.K., Kumar, S., Senguttuvan, T.D. and Gupta, B.K., 2022. Ultrasensitive Boron–Nitrogen–Codoped CVD Graphene-Derived  $\text{NO}_2$  Gas Sensor. *ACS Materials Au*, 2(3), pp. 356–366.

Niu et al. [104] described the process of developing Si-doped graphene nanosheets (SiGNSs) by annealing a mixture of GO and tetraethoxysilane (TEOS) at a high temperature ( $400\text{ }^\circ\text{C}$ ) in a closed glass ampoule. In order to detect  $\text{NO}_2$  gas, the doped Si atoms play an important role. The experiments for gas sensing were conducted between  $16$  and  $20\text{ }^\circ\text{C}$ . Even at  $\text{NO}_2$  gas concentrations as low as 1 ppb, SiGNS-400 had poor responses, revealing that SiGNS-400 has a low LOD for  $\text{NO}_2$  gas. The absolute response values increased with increasing  $\text{NO}_2$  gas concentration, as response values are shown by the line graph of the SiGNS-400 towards  $\text{NO}_2$  gas concentration. The response was found to be around 21.5 for 50 ppm  $\text{NO}_2$  gas concentration, and the response and recovery time were noted as 126 s and 378 s, respectively, at  $16\text{ }^\circ\text{C}$ . At certain temperatures, the sensor response values increased with an increase in  $\text{NO}_2$  gas concentration. Moreover, as the temperature increases, the sensor's response value to a concentration decreases. The results show that the SiGNS-400 sensor was more sensitive toward lower temperatures compared to higher temperatures. Further observed that since the response time reduced as the operating temperature increased, the response was faster at higher operating temperatures.

Singh et al. [105] show a portable microwave gas sensor was fabricated using a double split ring resonator (DSRR), and rGO is proposed. Two main steps are used to fabricate the sensor: the DSRR is produced on an FR-4 substrate and excited by a high-impedance microstrip line. The rGO is generated chemically and coated inside the DSRR's smaller ring. NO<sub>2</sub> gas with concentrations of 100–400 ppm is used to measure the sensor performance at room temperature. Since the gas molecules diffuse quicker for NO<sub>2</sub> than C<sub>2</sub>H<sub>5</sub>OH, the sensor responds more rapidly for NO<sub>2</sub> gas. Even at a very low concentration of 100 ppm, the rGO-DSRR sensor displayed good detection behaviour for NO<sub>2</sub> and C<sub>2</sub>H<sub>5</sub>OH gases. The response and recovery time of the sensor at room temperature to 100 ppm gas concentration were 71 s and 37 s, respectively. When compared to other sensors described in the literature, it was observed that the rGO-DSRR-based microwave sensor exhibits the shortest response and recovery time at RT for the detection of NO<sub>2</sub> and C<sub>2</sub>H<sub>5</sub>OH gases. Additionally, it showed that the sensor's overall sensitivity to the level of NO<sub>2</sub> is higher than its value as compared to the presence of C<sub>2</sub>H<sub>5</sub>OH gas. The higher electronegativity of NO<sub>2</sub> compared to C<sub>2</sub>H<sub>5</sub>OH gas is the main factor contributing to the NO<sub>2</sub> gas's increased sensitivity.

### (3) Hydrogen sulphide sensors

Choi et al. [106] said that electrospinning and high-temperature calcination were used to create 1D nonwoven tin oxide nanofibrous (SnO<sub>2</sub> NF) mats with a high surface-to-volume ratio. Then, the SnO<sub>2</sub> NFs and Graphene oxide nanosheets (GO NSs) were combined, and in the final stage, the GO NSs were reduced to rGO NSs by annealing in the gas-forming process. Figure 4 [106] represents the fabrication process of these sensors.

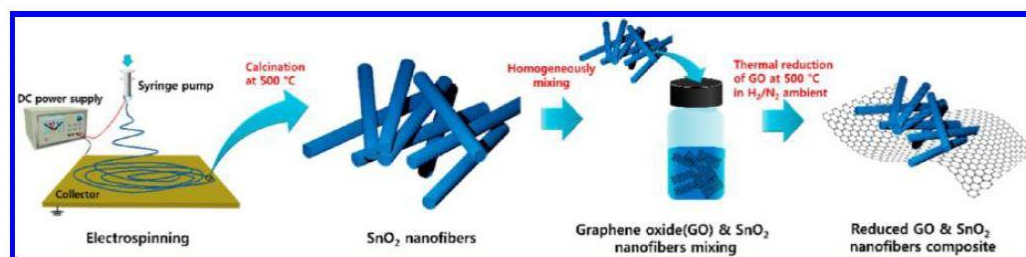


**Figure 4.** Representation of the fabrication process of the rGO/SnO<sub>2</sub>-based sensors for H<sub>2</sub>S gas detection [106]. Reproduced from Choi, S.J., Jang, B.H., Lee, S.J., Min, B.K., Rothschild, A. and Kim, I.D., 2014. Selective detection of acetone and hydrogen sulfide for the diagnosis of diabetes and halitosis using SnO<sub>2</sub> nanofibers functionalized with reduced graphene oxide nanosheets. *ACS applied materials & interfaces*, 6(4), pp. 2588–2597.

The sensor operating temperatures used for the gas sensing measurements ranged from 150 °C to 400 °C. The strongest response to H<sub>2</sub>S at 200 °C was shown by the 0.01 wt.% rGO NS-loaded SnO<sub>2</sub> NFs, which was 33.7 at 5 ppm, 7.6 times more than the response of the pure SnO<sub>2</sub> NFs at the same temperature, which was 4.4 at 5 ppm. The response of the H<sub>2</sub>S gas increased with an increase in temperature. Regarding H<sub>2</sub>S gas, it has been found that halitosis patients' exhaled breath has an odour-recognisably high concentration of H<sub>2</sub>S gas at 1 ppm, which is well within the detection range of H<sub>2</sub>S for the 0.01 wt.% rGO NS-loaded SnO<sub>2</sub> sensor.

Jiang et al. [107] explain that Fe<sub>2</sub>O<sub>3</sub>/graphene was successfully synthesized using a supercritical CO<sub>2</sub>-assisted thermal method, and paper-like nanosheets were created by vertically assembling individual Fe<sub>2</sub>O<sub>3</sub>/graphene nanosheets in a directed flow under the control of a controlled magnetic field. The later-produced VAFe/GN and HAFe/GN papers have great response characteristics to H<sub>2</sub>S gas with good selectivity in addition to good flexibility, indicating their potential usage as simple, inexpensive, and highly effective H<sub>2</sub>S gas sensors. In response to 23 ppm H<sub>2</sub>S gas at 190 °C, the HAFe/GN sensor shows CL emissions of roughly 350 absorption units. The more interesting is that the VAFe/GN paper device shows greater sensitivity than the HAFe/GN device. The acquired sensor also exhibits strong reproducibility with just slight differences for 4 replicate inputs of 15 ppm



H<sub>2</sub>S gas at 190 °C, a quick response time of 500 ms, and a short recovery time of about 30 s. Other gases, such as toluene, CO<sub>2</sub>, benzene and C<sub>2</sub>H<sub>5</sub>OH, were used to test the VAFe/GN paper sensor at temperatures ranging from 100 °C to 300 °C. None of these gases produced any measurable CL signals, indicating the sensor's excellent H<sub>2</sub>S gas selectivity.

#### (4) Ammonia sensors

Tanguy et al. [108] prepared nanocomposites of polyaniline (PANI) and nitrogen-doped reduced graphene oxide (N-rGO) with localized heterojunctions. In situ synthesis is used to strategically incorporate rGO nanosheets with electrical properties altered by N-doping into p-type PANI, with the nanosheets serving as templates for PANI growth. The N-rGO/PANI nanocomposites surpassed PANI and N-rGO alone in terms of ammonia gas sensing (at a concentration of 100 ppm), demonstrating the existence of a beneficial synergistic effect. The sensing response of PANI and N-rGO/PANI nanocomposite was measured over a range of ammonia gas concentrations (20–200 ppm) to evaluate their sensitivity and detection limit. At 0.5 wt.% N-rGO nanosheets loading, the maximum sensing response was obtained, and as the nanosheets loading level increased, the sensing response decreased. The developed N-rGO/PANI nanocomposite demonstrated its outstanding suitability for the design of tiny, high-efficiency, robust, and inexpensive sensors with superior sensing performance achieved. This is true for applications in monitoring food freshness as well as for routine testing of traces of volatile amines in medical, environmental and health, and industrial applications. Sett et al. [109] showed by using a modified version of Hummer's process, and graphite powder was chemically separated to create GO. A transparent sheet was used to fabricate the sensor. To maintain the transparency sheet's durability throughout the photolithographic process, it was thermally treated at 80 °C. The rGO sensor's ammonia sensing properties were discovered at room temperature. The best-optimized test that was used in subsequent experiments was the 16 h rGO. The sensor exhibits an 80% response towards 10 ppm ammonia and a 930% response to 400 ppm ammonia. Due to adequate functional group modification, the sensor displays almost complete recovery to its baseline. The sensor has a full recovery and has high repeatability. At an ammonia concentration of 400 ppm, the response and recovery time are 31 s and 500 s, respectively. Temperatures ranging from 25 °C to 100 °C were used for the sensing. Due to the repetition in desorption at higher temperatures, the sensor responds poorly after 70 °C. The sensor operates most well between 25 and 55 °C.

Ahmed et al. [110] mentioned that pure graphene monolayer dispersion was bought from the Graphene Supermarket Company. The mixture has been deposited on a ceramic surface. By depositing Au (60 nm) electrodes onto the substrate, the ohmic contact was built. It has been demonstrated that as soon as the exposure stops, the resistance begins to increase rapidly. After 5 min, the resistance tends to level off and achieve its highest level. Ammonia functions as an acceptor and removes electrons from the graphene sheet, as shown by the increase in resistance. The highest response was nearly 200 s, and this result is extremely consistent with other data that have been published. Since the response of graphene to NH<sub>3</sub> gas varied from 100 to 1000 s; these results are comparable to those of other studies that have been published. Srivastava et al. [111] said low-pressure chemical vapour deposition (LPCVD) had been employed to develop boron-doped few-layer graphene (BFLGr) via an easy procedure. A Si/SiO<sub>2</sub> substrate with gold-patterned electrodes was employed to fabricate the gas sensing device. PFLGr and BFLGr sensors were exposed to NH<sub>3</sub> gas concentrations ranging from 16 to 256 ppm at various levels. Compared with the PFLGr sensor, the BFLGr sensor has a higher response and faster recovery. For 32 ppm of gas, the response rates for the PFLGr and BFLGr sensors were 2.64% and 8.92%, respectively. The BFLGr sensor's calculated response time was 0.85 s, which was considerably less than the undoped PFLGr sensor was 3.56 s, and the sensors' recovery times were 36.3 s and 48.2 s, respectively. The sensors were exposed to 256 ppm of NH<sub>3</sub> gas to evaluate the repeatability and reproducibility, and three response-recovery cycles were recorded. The sensors' excellent level of repeatability and reproducibility for continuous gas exposure and maintenance of response was clearly observed.

### (5) Ethanol sensors

Tian et al. [112] showed that  $\text{Co}_3\text{O}_4$  and rGO nanosheets were used to fabricate layer-by-layer nanocomposites by an easy hydrothermal procedure that included an annealing step. A tiny alumina tube with two Pt electrodes was covered with the composite materials in their as-fabricated condition. As the operating temperatures increased from 150 °C to 200 °C, the sensor sensitivity improved.  $\text{Co}_3\text{O}_4$  and CGO 15% sample's optimal working temperatures were 220 °C and 200 °C, respectively. The sensor responses are based on a GCO 15% sample and pure  $\text{Co}_3\text{O}_4$ . The sensors' sensitivity increased as the  $\text{C}_2\text{H}_5\text{OH}$  gas concentration increased. When the temperature reached 200–220 °C, the sensing responses first increased to their highest levels, but as the temperature increased, they also slightly declined, likely as a result of the changing oxidation ability of the adsorbed oxygen. The sensor with the best response to the  $\text{C}_2\text{H}_5\text{OH}$  vapour operating at 200 °C was based on a 15% GCO sample.

Rafiee et al. [87] reported ZnO NWs were developed by conducting the crystalline deposition of ZnO NWs on Gr nanosheets using a simple hydrothermal technique. The Gr/ZnO NWs nanocomposite that was developed was investigated as a potential sensing material. The response toward 20 ppm of  $\text{C}_2\text{H}_5\text{OH}$  vapour was measured as a function of working temperature to investigate the gas sensing characteristics of both ZnO NWs and Gr/ZnO NWs sensors. It was found that the responses for the Gr/ZnO NWs and ZnO NWs initially improved with temperatures up to 200 °C and 125 °C, respectively, and degraded at higher temperatures. In order to examine the gas sensing properties of ZnO NWs and Gr/ZnO NWs sensors, respectively, the optimal temperatures of 200 °C and 125 °C were chosen in order to examine gas sensing properties of ZnO NWs and Gr/ZnO NWs sensors, respectively. It was clear that as the  $\text{C}_2\text{H}_5\text{OH}$  concentration increases in both sensors, the sensors' sensitivity to the  $\text{C}_2\text{H}_5\text{OH}$  vapour increases. The Gr/ZnO NWs sensor had the highest response of 26 to 1 ppm at 125 °C temperatures. Husain et al. [113] employed anhydrous  $\text{FeCl}_3$  as the oxidizing and doping agent while using in situ chemical oxidative polymerization to synthesize PTh and PTh/G in the presence of various amounts of graphene nanosheets in chloroform. Each sample was turned into a pellet, which was then attached to four probes and stored in a chamber with  $\text{C}_2\text{H}_5\text{OH}$  vapours. The pellet remained for 60 s in the presence of  $\text{C}_2\text{H}_5\text{OH}$  vapours. For PTh and PTh/G-3, the sensing response was evaluated with respect to changes in DC electrical conductivity. The surface area of nanocomposites increases along with the deposition of graphene nanosheets in PTH. For  $\text{C}_2\text{H}_5\text{OH}$  concentrations of 2000 ppm, the highest sensing response as a function of electrical conductivity change was observed. Sensing response also increases when  $\text{C}_2\text{H}_5\text{OH}$  gas concentrations increase from 400 to 2000 ppm.

Fauzi et al. [114] described that by using the Tour's approach to oxidize and exfoliate expanded graphite, GO nanosheets are created. By vacuum filtering, GO nanosheets are stacked to create GO membranes. Due to the exceptional activity of gold nanoparticles for the catalysis of organic molecules, Au-loaded  $\text{WO}_3$  is utilized as the sensing electrode. At all temperatures, the sensor responded to changes in the  $\text{C}_2\text{H}_5\text{OH}$  gas concentration in the air. At 25 °C, the sensor's response was the highest. However, when the operating temperature increases, the sensor response decreases. As the thickness decreases, the sensor's response increases. Additionally, by reducing the thickness, the response time was increased. TPD studies had shown that the reduced sensor response was caused by the effective combustion of  $\text{C}_2\text{H}_5\text{OH}$  gas in the thick sensing layer. The current sensor's poor response and recovery time was by far its biggest flaw.

#### 3.2. Graphene Quantum Dots-Based Gas Sensors

GQDs consist of a monolayer or a few monolayers of graphene-related to quantum confinement and edge effects [115]. These materials offer enhanced qualities, such as intense fluorescence activity, chemical inertness, photostability, tunable low cytotoxicity, luminescence emission, outstanding biocompatibility, high solubility, enduring opposition to photobleaching, superior surface area, and improved surface grafting [116,117]. These

properties are unique for offering the opportunity to explore novel structural, optical and electrical phenomena inaccessible in other materials. The modification of electron and quantum confinement behaviour for GQDs has become enormously appealing, especially in contrast to graphene. These sophisticated properties make this material a promising candidate for numerous applications such as biosensors, sensors, photovoltaic, bioimaging, energy storage devices etc. [118,119]. GQDs demonstrate outstanding solubility in organic solvents such as tetrahydrofuran (THF), acetone, dimethylformamide (DMF), dimethyl sulfoxide (DMSO) and C<sub>2</sub>H<sub>5</sub>OH gas [120].

Before getting the material to the application, material synthesis is the most important and foremost. GQDs are formed from carbon-rich materials such as glucose, fullerene, GO, graphite, CNTs and carbon fibres (CFs), which are pioneers. Top-down and bottom-up approaches are followed for synthesizing the GQDs. It is challenging to have such kinds of complicated synthesis techniques for the conventional semiconductor quantum dots [121]. The controllable synthesis is a precise but complex mechanism, requiring numerous processing steps for achieving GQDs with a large aspect ratio. GQDs are achieved with appropriate small molecules or polymers via dehydration while using the carbonization method. These manufacturing procedures are usually not controllable, leading to the aspect ratio heterogeneity for GQDs. The commendable aspect is that the GQDs are biocompatible due to non-toxic reagents. As per the existing knowledge, most of the top-down synthesis approach involves the cleavage of carbonaceous material. However, these methods have considerable shortcomings concerning unexpected damage to the structure, low yield, and non-uniform morphologies [122–124]. As it is known that the GQDs have a unique structure and excellent properties, the main top-down approaches designated are a hydrothermal or solvothermal method, oxidative cleavage ultrasonic-assisted process, microwave-assisted process, CVD, pulsed laser ablation (PLA) electrochemical oxidation, and electrochemical method [125–132]. On the other hand, the bottom-up approaches introduce controllable synthesis and carbonization. The synthesized GQDs have strong luminescence emission, a good size range, and satisfactory properties [133–139].

#### a. Carbon dioxide sensors

Raeyani et al. [140] reported a novel graphite intercalation compound hydrothermally prepared optical gas sensor based on GQDs. Due to the lack of various chemicals and the use of the simple drop-casting approach, both synthesis and sensor fabrication procedures are very affordable and simple to prepare. It was observed that at 310 nm, the relative absorbance increases when CO<sub>2</sub> is exposed and returns to the initial state when the gas is removed from the chamber. At 100 ppm, said to be the lowest concentration, which was tested, the GQDs exhibited great sensitivity. This was also repeated at 260 nm, and a similar outcome was obtained. When air and gas were exposed, optical absorption intensity was lower at shorter wavelengths than it did at longer wavelengths. As a result, shorter wavelengths have a weaker sensing response than longer wavelengths. For 1000 ppm of CO<sub>2</sub> gas, the computed response in the wavelength of 310 nm was approximately 50%, and for concentrations of 500, 300, and 100 ppm, it was approximately 40%, 8%, and 4%, respectively. GQDs sensor films exposed to CO<sub>2</sub> gas at room temperature demonstrated a considerable optical absorption change. The response at 260 nm was significantly lower than what was observed at 310 nm. The response and recovery time of the sensor were around 106 s and 150 s, respectively. The high and partial reversible responses were observed, showing the potential application as an optical gas sensor for the detection of CO<sub>2</sub> gas.

#### b. Nitrogen dioxide sensors

Song et al. [141] built a flexible graphene electrode layer with a crumpled quantum dot (QD) sensor layer on an elastomeric substrate. Due to their superior gas-sensing capabilities and solution-processability, PbS CQDs were chosen because they allow for the adhesion-rich deposition of room-temperature films on soft substrates. The sensor was exposed to a different gas concentration ranging from 10 to 150 ppm. The sensor's response increased with an increasing gas concentration in the range of 1–150 ppm, with a saturation tendency at higher

concentrations. The relying of the sensor response on the NO<sub>2</sub> gas concentration in the range of 1–20 ppm was roughly linear. The calculated limit of detection (LOD) was approximately 13 ppb. The champion sensor showed outstanding NO<sub>2</sub>-sensing selectivity against C<sub>2</sub>H<sub>5</sub>OH vapour, H<sub>2</sub>S, NH<sub>3</sub> and SO<sub>2</sub> at room temperature, as well as a high response sensitivity of 125.0 toward 50 ppm NO<sub>2</sub> gas with a response and recovery times of 7 s and 22 s, respectively. Jiang et al. [142] described that a hybrid material was composed using metal phthalocyanine derivatives and GQDs. Modified Hummer's method was used for the preparation of GO, and the sensor was fabricated using the drop cast technique. The response values of CoPc-GQDs hybridization sensing devices gradually increase when the O-GQD heating temperature increases from 100 °C to 700 °C. The faster response time of metal phthalocyanine is promoted by the GQDs' enhanced conductivity. The lowest acceptable response concentration was 50 ppb. The consistent results showed that using the laser-aided irradiation approach, all three devices exhibit excellent NO<sub>2</sub> gas reversibility. The sensor response value to 50 ppm NO<sub>2</sub> gas at room temperature was 15.8, and the obtained response and recovery time were 1.67 s and 1.67 s, respectively. At low concentrations, CoPc-response G-00's value also significantly improved.

Zhang et al. [143] said that the hydrothermal approach was used to successfully prepare the N-GQDs modified ZnO composite material at 160 °C for 4 h. the linear relationship in a 5 ppm NO<sub>2</sub> atmosphere between the operating temperature and the gas sensing response. The outcome indicates that 160 C is the ideal operating temperature for pure ZnO. The best operating temperature for N-GQDs was reduced to 100 °C after modification, and the sensitivity was substantially increased. At low temperatures, the G-Z-2-based sensor exhibits remarkable NO<sub>2</sub> gas sensitivity. The adsorption capacity of N-GQDs on NO<sub>2</sub> gas diminishes with temperature, which lowers the sensing performance at high temperatures. Under the condition of 100 °C, the sensing characteristics of ZnO and N-GQDs/ZnO composites to 5 ppm NO<sub>2</sub> gas were further studied. G-Z-2 (58) responded to NO<sub>2</sub> gas 11.6 times more strongly than ZnO. A 30-day stability test on ZnO and G-Z-2 demonstrates G-Z-2's outstanding stability. The gas sensitivity test of 5 ppm various gas at 100 °C demonstrates G-Z-2's selectivity to NO<sub>2</sub>. The benefits of heterojunction, active N atom doping, and oxygen vacancy are mostly responsible for the outstanding sensing performance of G-Z-2.

### c. Hydrogen sulphide sensors

Nan Li et al. [144] created a GQD-based (2,4-dinitrophenoxy)-tyrosine (DNPTYR) functionalized fluorescence turn-on probe for H<sub>2</sub>S gas. Pyrene (C<sub>16</sub>H<sub>10</sub>) was used as the carbon precursor in the simple hydrothermal synthesis of GQDs in sodium bicarbonate (NaHCO<sub>3</sub>) solution, which was followed by neutralizing the excess acid and dialysis. In response to NaHS, GQD-PL DNPTYR's intensity varies in a dose-dependent manner. Due to the low levels of H<sub>2</sub>S gas in our bodies, such as those seen in brain and liver tissues at 15 nanomolar levels, the high sensitivity obtained by our sensor was crucial. Testing the GQD-DNPTYR probe (0.05 mg/mL) for H<sub>2</sub>S gas selectivity with a variety of biologically important species was conducted. Since thiolysis of dinitrophenoxyl ether under a physiological pH of 7.4 is significantly more sensitive to H<sub>2</sub>S gas than other free thiols and anions, the GQD-DNPTYR probe exhibits such remarkable selectivity.

### d. Ammonia sensors

Hakimi et al. [145] mentioned that on a transparent substrate, the gas sensors were employed using a conductive polymer and N-GQDs dopant at room temperature. The silver conductive paste was applied for external circuit contact, and the drop cast technique was used for the deposit of the sensitive film. To examine the impact of N-GQD on the sensing response, various amounts of the substance were added. The results demonstrated that the addition of N-GQDs significantly improved the sensing response. The sensor response decreases with an increase in temperature. Room temperature was found to be the ideal working temperature. When the response to NH<sub>3</sub> gas was compared with the selectivity of the N-GQDs/PEDOT-PSS sensor to 1500 ppm of toluene, acetone, C<sub>2</sub>H<sub>5</sub>OH, and CO<sub>2</sub>, it demonstrates the sensor's high selectivity to NH<sub>3</sub> gas. The incorporation of N-GQDs dopant to PEDOT-PSS enhanced the sensor's properties. When NH<sub>3</sub> gas was exposed to 1000 ppm, the response was noted as

116.38%, and the response and recovery time were recorded as 7.7 and 10 min, respectively. The composite N-GQD and PEDOT-PSS sensor had higher stability than a sensor only using PEDOT-PSS. Arunragasa et al. [146] mentioned hydrothermal method was used for the synthesis of OH-GQDs. The drop casting technique was used for the fabrication of hydroxyl functionalised graphene quantum dots on an interdigitated nickel electrode. This was said to be an alternative gas sensor at room temperature. The sensor response at different concentrations of  $\text{NH}_3$  gas ranging from 10 to 500 ppm was noted at room temperature. When the sensor is exposed to  $\text{NH}_3$  gas, the resistance decreases quickly and the recovery to the initial value when exposed to air. The response of the OH-GQDs sensor was found to be increasing linearly in the concentration ranging between 10 and 500 ppm. At 500 ppm  $\text{NH}_3$  gas, the OH-GQDs sensor's estimated response and recovery time were 64 and 69 s, respectively. High  $\text{NH}_3$  gas sensitivity and quick response and recovery times are exhibited by the OH-GQDs sensor. By exposing the OH-GQDs gas sensor to various environment gases and volatile organic compound vapours, the sensor's selectivity was evaluated, and it was clear that the OH-GQDs gas sensor responds more strongly toward  $\text{NH}_3$  gas, demonstrating a high selectivity.

Wongrat et al. [147] elaborated that GQDs materials are decorated onto a ZnO surface to create p-n heterojunctions. This results in a change in the surface chemical reactions at the junction of the symmetrically paired materials. The sensor samples were fabricated onto a quartz tube to build  $\text{NH}_3$  gas detecting systems. ZnO: GQD heterojunctions are important candidate materials due to their extremely selective sensitivity to  $\text{NH}_3$  vapour. Specific  $\text{NH}_3$  concentrations were varied in the range of 1–1000 ppm at room temperature (27 °C) and relative humidity of 65 RH% to record the gas response data. The sensors' resistances dramatically decreased when exposed to an  $\text{NH}_3$  atmosphere. The resistance increased quickly to almost its initial amount when the  $\text{NH}_3$  vapour was withdrawn from the system. As the  $\text{NH}_3$  concentration increased, the sensors based on pure ZnO and ZnO: GQDs responded more strongly. The responses of the ZnO and ZnO: GQDs sensors were routinely monitored while being exposed to  $\text{NH}_3$ ,  $\text{C}_2\text{H}_5\text{OH}$ , acetone, and water to ascertain their selectivity. The sensors developed on ZnO: GQDs were found to have the best  $\text{NH}_3$  vapour selectivity. Hong et al. [148] described the production of N-doped graphene quantum dots (N-GQDs) by a hydrothermal procedure by electrostatic interaction and were coated on hollow indium trioxide ( $\text{In}_2\text{O}_3$ ) nanofibers made via an efficient combination of electrospinning and high-temperature calcination. Figure 5 [148] shows the schematic diagram of the sensing mechanism of these prototypes.

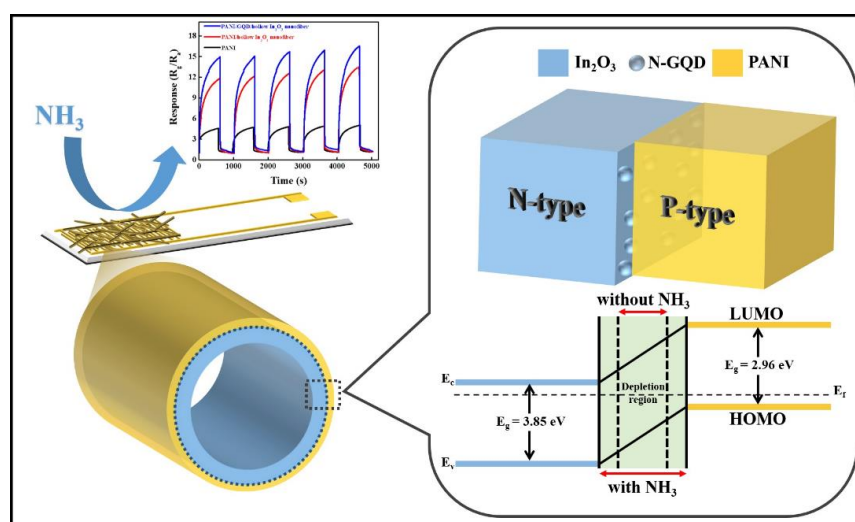


**Figure 5.** Representation of sensing mechanism of the N-doped GQDs for  $\text{NH}_3$  gas detection. Reproduced from Hong, S.Z., Huang, Q.Y. and Wu, T.M., 2021. The room temperature highly sensitive ammonia gas sensor is based on polyaniline and nitrogen-doped graphene quantum dot-coated hollow indium oxide nanofiber composite. *Polymers*, 13(21), p. 3676 [148].

The nanofiber sensor was designed to find  $\text{NH}_3$  gas in a concentration range from 0.6 ppm to 2.0 ppm at ambient temperature to determine the sensing performance of the composite sensor fabricated for the analysis of human breath and kidney diseases. When the sensor was exposed to  $\text{NH}_3$  gas of 1 ppm at room temperature, it was found that when the sensor reacted with the gas, a change in resistance was observed and returned to the initial state when it was exposed to air. The results showed that the composite film has remarkable performance and great reversibility of the nanofiber sensor. The PANI/hollow  $\text{In}_2\text{O}_3$  nanofiber sensor is said to have a higher response value when compared with pure PANI. The response value of pure PANI was around 3.6, whereas the composite with 20 wt.% loading was 11.2, and PANI/N-GQD/hollow  $\text{In}_2\text{O}_3$  had a response value of 15.6. When the concentration of the gas increases, the response also increases. PANI/N-GQD/hollow  $\text{In}_2\text{O}_3$  nanofiber sensor is said to exhibit the highest response. QGDs have progressed as sensor materials due to the availability of more edge atoms than 2D materials, where more adsorptions occur because of the surface atoms [149]. Chen et al. [150] synthesized two different GQDs (neutral and acidic) and developed them for fabricating  $\text{NH}_3$  gas sensors. The characteristic studies of sensors A and B (neutral and acidic) were examined with the exposure to different concentrations of  $\text{NH}_3$  gas, as shown in Figure 6 [151].

The current responses were  $-14.9\%$  and  $5.9\%$  when the sensors were exposed to  $\text{NH}_3$  gas (Figure 6a,b). It was indicated that the sensors have different electrical responses with the same concentration of the gas molecules. The sensors are highly stable (Figure 6c,d), and the response and recovery can be varied (Figure 6e,f) to different  $\text{NH}_3$  concentrations. Additionally, the absolute response of the sensors at various concentrations is shown in Figure 6g, while the ones made with aqueous GQDs with pH 7 and pH 5, respectively, are shown in Figure 6h.

#### e. Ethanol sensors

Rahimi et al. [151] discussed that GQDs was easily created by pyrolyzing citric acid and then GQDs were placed onto the thin ZnO NR film, and zinc oxide nanorods (ZnO NRs) were formed on pre-seeded glass substrates using a solvothermal process. It was observed that the GQDs' incorporation reduced the ZnO NR thin film's photoluminescence (PL) intensity. Compared to bare ZnO NR thin film, the GQD-ZnO NR thin film has a much higher sensitivity. As the number of sensing cycles grows, the maximum sensitivity of the bare ZnO NR thin film slightly increases, while it is observed that the highest sensitivity of the GQD ZnO NR thin film gradually falls and approaches a slightly uniform condition. The sensitivity of ZnO NR thin film to  $\text{C}_2\text{H}_5\text{OH}$  gas was dramatically increased by the addition of GQDs. In comparison to its resistivity in the vacuum, ZnO exhibits a greater resistance when the atmosphere is present.

Another work, as shown by S. Shao et al. [152], highlights the development of gas sensors using GQD-functionalized porous and hierarchical  $\text{SnO}_2$  quantum nanoparticles via a self-assembly strategy. The prototypes consisting of the interdigital electrode were treated with a self-assembled technique to embed  $\text{SnO}_2$  QNP/ZnO nanosheets on them. A post-synthetic humidity treatment was then carried out to construct the GQDs and  $\text{SnO}_2$  QNP-loaded ZnO nanosheets hetero structures. Some of the advantages of these sensors were their high reproducibility and control of structure formation. The change in resistance occurred because of a strong synergistic effect and p-n heterojunction occurring between the p-type GQD and n-type  $\text{SnO}_2$  and ZnO. This synergistic effect took place due to the change in the degree of adsorption of oxygen molecules. As compared to the pure ZnO and  $\text{SnO}_2$ /ZnO sensors, the GQD-modified hierarchical  $\text{SnO}_2$  QNP/ZnO nanostructured devices exhibited certain attributes, such as excellent response with a sensitivity of 15.9 for 0.1 ppm  $\text{H}_2\text{S}$  gas, fast response, and recovery times of 14 s and 13 s, respectively, and high selectivity toward  $\text{H}_2\text{S}$  gas with respect to other interfering gases. When the principal component analysis (PCA) technique was also deployed to analyze the sensing performance of these hierarchically structured devices, the combined effects of GQD/ $\text{SnO}_2$  QNP/ZnO hetero interfaces for the improvement of the selectivity of the sensors were

realized. The GQD-modified SMO with the hierarchical structure depicted their higher potential to perform non-invasive exhaled diagnosis.

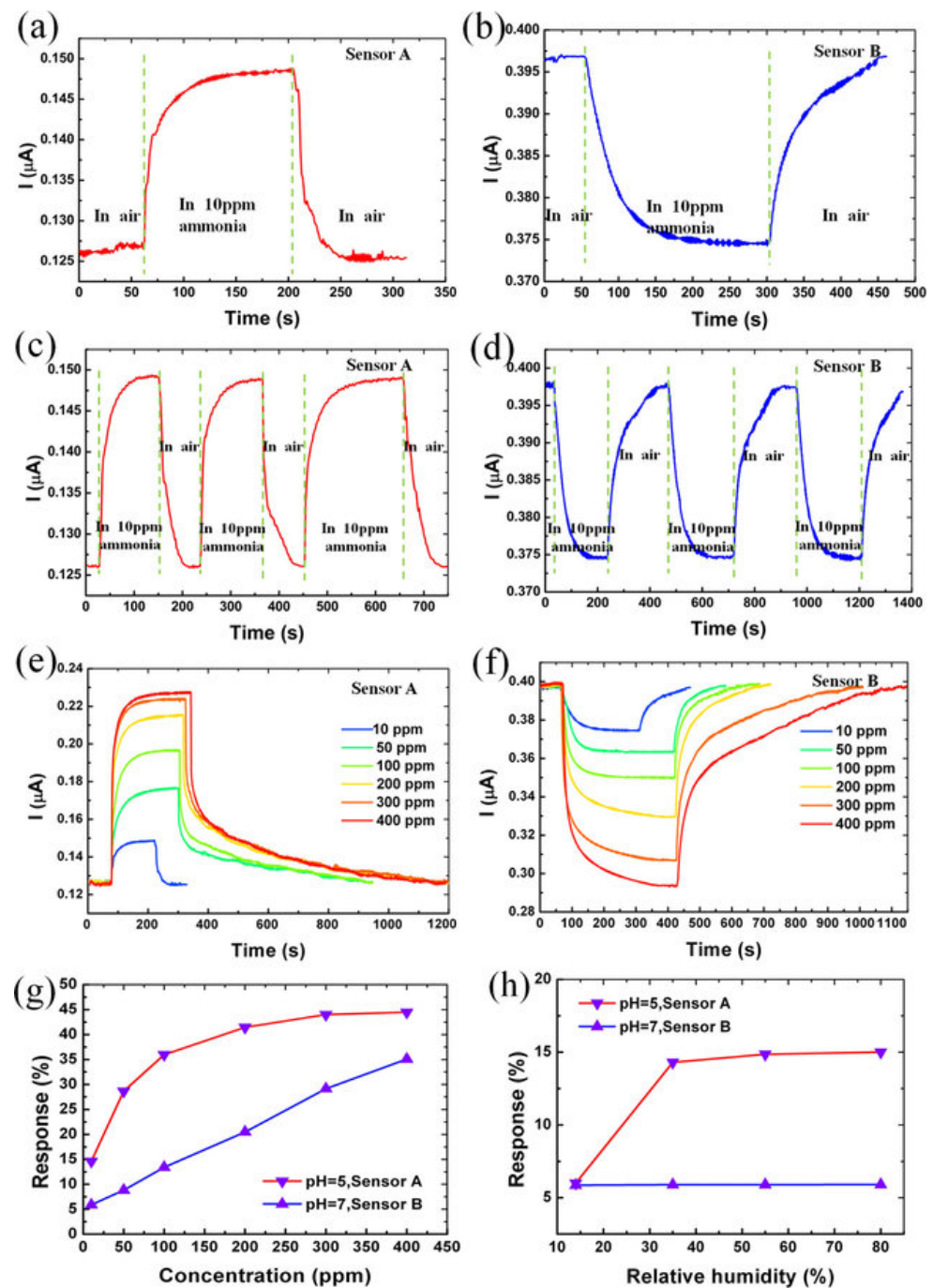


**Figure 6.** (a,b) 10 ppm NH<sub>3</sub> gas response characteristic of sensors A and B, respectively. (c,d) Response of sensors A and B to 10 ppm NH<sub>3</sub> gas for three cycles, respectively. (e,f) Current response behavior for sensors A and B at different concentrations of NH<sub>3</sub> ambience (g) absolute response of sensors A and B at various concentrations of NH<sub>3</sub> gas (h) absolute response of sensors A and B to 10 ppm NH<sub>3</sub> gas at various relative humidity. Reproduced from Rahimi, K. and Yazdani, A., 2018. Ethanol-sensitive nearly-aligned ZnO nanorod thin films covered by graphene quantum dots. *Materials Letters*, 228, pp. 65–67 [151].

### 3.3. Reduced Graphene Oxide-Based Gas Sensors

Similar to the other types of graphene forms, rGO has been equally responsible for detecting multiple gases at different concentrations. The advantages of rGO as compared to graphene, rGO has higher dispersion in water and other organic solvents. It can also be used as a semiconducting and insulating material due to the disruption in the  $sp^2$  bonding networks. Due to their large surface-to-volume ratio, a higher degree of adsorption and catalytic activity takes place on rGO-based as compared to the other graphene-based sensors [153].

#### a. Carbon dioxide sensors

Zhou et al. [154] employed rGO films alongside ZnO film as supporting material using the sol airbrush technique. Two thin films were fabricated, rGO was applied directly to the film, and ZnO was used as supporting material. The SEM images showed that the surface of the rGO-ZnO film was rougher when compared with only rGO film. As more rGO solution was added to the lower range of concentrations (1000 ppm–3000 ppm), the sensitivity increased. An increase in the film thickness exhibited a high sensitivity in the 4000–7000 ppm concentration range. The rGO/ZnO film sensor responded in 10 s to 15,000 ppm  $CO_2$ , whereas the single layer rGO film sensor takes about a minute. Zhou et al. [155] used the hydrothermal method to prepare a rGO/N-MXene composite solution. Patterns were created using the lithography technique on a silicon substrate. Later, the targeted solutions were coated using a spray coating. The results show that the sensor response increases with higher  $CO_2$  gas concentration. The ternary sensor (rGO/N-MXene/PEI) was used to detect  $CO_2$  gas with a range of 4–3000 ppm under 62% relative humidity. As a function of operation temperature (20, 30, 40, and 50 °C), the ternary sensor was successively exposed to 40 ppm  $CO_2$  gas under 62 RH%. The response occurred maximum across all conditions at 20 °C, with full recovery. The sensor is said to reveal reversible and sensitive to  $CO_2$  gas detection.

Hafiz et al. [156] prepared rGO using hydrogen plasma reduction. The fabrication process was carried out by spin-coating GO solution on a patterned Si. For the sensor rGO-F20, the pressure was maintained at 0.30 mbar and had a hydrogen flow rate of 20 sccm. The radio frequency was altered to decrease the sputtering and bombardment effect to reduce the formation of porous and rough rGO. The gas concentration ranged from 0 to 1500 ppm. It was found that the sensing response continuously increased with the increase in gas concentration. The sensor showed good response and repeatability, especially for indoor gas monitoring. When  $CO_2$  gas is exposed to 750 and 769 ppm concentrations, the sensor exhibits good repeatability performance with a sensing and recovery time of around 4 min. Without using any external recovery, the repeatability performance was evaluated in an air environment with 68 RH%. Gupta et al. [157] carefully examined how the concentration of the reducing agent affects the oxygen functional groups and how that affects the  $CO_2$  gas sensing. GO was primarily prepared by ultrasonication to obtain a uniformly dispersed solution. Ascorbic acid with different concentrations was added to the solution and heated at 65 °C. Changing the brown colour to blank colour signifies the formation of rGO. Quartz crystal microbalance (QCM) was used as substrate material. Later a drop-casting technique was used to prepare a thin film for gas sensing. It was found that all of the AArGO-coated QCM sensors responded significantly, continuously, and repeatedly to  $CO_2$  gas (50 ppm or 500 ppm) at room temperature. For  $CO_2$  at room temperature at 500 ppm and 50 ppm, the functionalized AArGO25 gas sensor exhibits recordable high sensing qualities (response and recovery time) with good repeatability. With a sensitivity of 50 Hz/g, a quick response and recovery time of 26 s and 10 s, respectively, are attained for 500 ppm  $CO_2$  gas. The response/recovery time for AArGO50 and AArGO100-based sensors were measured to be 40 s/39 s, 52 s/30 s for 500 ppm  $CO_2$  gas and 46 s/47 s, 58 s/35 s for 50 ppm  $CO_2$  gas. Though these sensors show a good response to  $CO_2$  gas, they do not desorb completely during recovery.



## b. Nitrogen oxide sensors

Galstyan et al. [158] developed a hybrid structure using ZnO and GO nanostructure. Radio Frequency (RF) magnetron sputtering was used to deposit Zn thin films on SiO<sub>2</sub> and alumina substrates. The process of developing rGO/ZnO composites by fusing GO sheets to ZnO nanostructures and then thermally reducing GO at 250 °C in an argon gas system. Temperatures ranging from room temperature to 250 °C were used for the measurements. The pure ZnO and rGO/ZnO composite were exposed to NO<sub>2</sub> gas with different concentrations (1 ppm, 2 ppm, and 5 ppm) at 200 °C with RH at 40%. The better sensing results were obtained in the range of 200–250 °C temperature. The responses of ZnO and rGO/ZnO were higher at 250 °C when compared with at 200 °C. When exposed to 5 ppm NO<sub>2</sub> gas, rGO/ZnO sensors had a sensor response of 5.4, which is about 1.4 times more than that of ZnO sensors obtained under the same operating parameters. Wang et al. [159] used the sol-gel method to synthesize the SnO<sub>2</sub>/rGO composite. In brief, the GO was synthesized using a modified Hummer's process from powdered natural graphite. Epichlorohydrin (PPD) and SnCl<sub>4</sub>·5H<sub>2</sub>O were slowly added to the GO/DMF solution and stirred. After a few days of solution exchange, the SnO<sub>2</sub>/rGO composite was formed, dried, and carbonized for two hours at 600 °C in an argon atmosphere. The performance of the SnO<sub>2</sub>/rGO composite sensors to detect gases was tested. The outcome shows that the SnO<sub>2</sub>/rGO composite, when compared to other gases, has a high selectivity to NO<sub>2</sub> gas. The SnO<sub>2</sub>/rGO was exposed to NO<sub>2</sub> gas at 750 ppb at an operating temperature from 33 to 189 °C. The relative responses of the sensor decrease with the increase in temperature, whereas the response time and recovery time decreases with the temperature increase. The response and recovery time of NO<sub>2</sub> gas 750 ppb are 7 s and 31 s, respectively, at a temperature of 189 °C. When the working temperature is reduced to 116 °C, the NO<sub>2</sub> gas sensor's response and recovery time increase to 17 s and 90 s, respectively. The optimal working temperature was determined to be 116 °C by considering the response time, recovery time, and the relative response of NO<sub>2</sub> gas sensors.

Zhang et al. [160] used hydrothermal synthesis to form porous Co<sub>3</sub>O<sub>4</sub> nanoparticles. A typical technique for synthesizing the Co<sub>3</sub>O<sub>4</sub>/rGO hybrid was treated where Co<sub>3</sub>O<sub>4</sub> is added with deionized water to form a homogeneous solution, then heated at 90 °C and centrifuged. Later it was frozen at −40 °C to obtain the black powder. A homogeneous paste was prepared with the above-mentioned powder and coated on an alumina ceramic tube to form a sensing film. The sensor based on undoped Co<sub>3</sub>O<sub>4</sub> at 100 °C obtained a response of 11.8% to 5 ppm of NO<sub>2</sub> gas. The sensors based on 1.0 wt.% and 2.4 wt.% rGO-Co<sub>3</sub>O<sub>4</sub> showed increased responses of 19.5% and 26.8% to 5 ppm of NO<sub>2</sub> gas at substantially lower optimum working temperatures of 65 °C and 25 °C, respectively. The resistance decreased when rGO-Co<sub>3</sub>O<sub>4</sub> was exposed to NO<sub>2</sub> gas. The undoped Co<sub>3</sub>O<sub>4</sub> is said to have a short response time and recovery time of 3.5 min and 1 min, respectively. The response time of 1.0 wt.% and 2.4 wt.% rGO-Co<sub>3</sub>O<sub>4</sub> were 4.5 min and 1.5 min. It was noted that the sensor response increases as the NO<sub>2</sub> concentration increases. The 2.4 wt.% rGO-Co<sub>3</sub>O<sub>4</sub> was chosen to further examine other gas sensing features after 2.4 wt.% of graphene was determined to be the optimal doping concentration after taking both gas response and optimal operating temperature into consideration. Zijiong Li et al. [161] showed that CuO/rGO nanohybrids could be synthesized in an easy one-pot method at room temperature by simultaneously forming CuO nanostructures and reducing GO. CuO/rGO nanohybrids were fabricated on a Si/SiO<sub>2</sub> wafer. At room temperature, the sensing performance of the sensors is as-fabricated to detect lower gas concentrations of NO<sub>2</sub> gas from 1 to 75 ppm. The response for NO<sub>2</sub> gas at 1 ppm is approximately 14, demonstrating outstanding gas sensitivity. When the response reached 90% of the total current change, the response time and recovery time were around 66 and 34 s, respectively. The response value increased from 14 for 1 ppm to 51.7 for 75 ppm as the NO<sub>2</sub> gas concentration increased. The response time and recovery time for 75 ppm NO<sub>2</sub> gas were around 50 s and 105 s, respectively, as the NO<sub>2</sub> gas concentration increased. CuO/rGO and pure CuO gas sensors show outstanding response

behaviour as the temperature increases. However, it was found that as the temperature reached 135 °C, the sensitivity of the CuO/rGO sensor began to drop.

### c. Hydrogen sulphide sensors

Song et al. [162] used the one-step colloidal synthesis method, where it was simple to regulate the reaction time to control the morphology of SnO<sub>2</sub>. The sensor was fabricated using the spin-coating technique at room temperature. When H<sub>2</sub>S gas was released, it was observed that SnO<sub>2</sub>/rGO were sensitive to 50 ppm at 22 °C. The sensor resistance decreased when H<sub>2</sub>S gas was released. The optimal sensor response to 50 ppm of H<sub>2</sub>S gas is 33 in 2 s, and it is completely reversible. Based on the H<sub>2</sub>S gas concentration, the response time was 2–13 s, showing good dynamic response and recovery capabilities at room temperature. At room temperature, the sensor responded to other gases at 50 ppm and suggested that H<sub>2</sub>S gas has better selectivity against other gases.

Chu et al. [163] used a one-step hydrothermal synthesis process at 180 °C for 15 h. SnO<sub>2</sub> particles were easily formed on the surface of rGO sheets to create the SnO<sub>2</sub>-rGO nanocomposite. The sensor was fabricated using a drop-casting technique, dispersing the nanomaterials on a ceramic plate. The responses of the sensor towards 100 ppm H<sub>2</sub>S gas were noted with different temperatures. At 50 °C, the response was 20.87% and returned to initial resistance after 45 min. The response increases with an increase in temperature and obtains a maximum value at 125 °C and then decreases gradually. By considering the responses and recovery time, 125 °C was considered the optimal operating temperature for the SnO<sub>2</sub>-rGO sensor. At 125 °C for 100 ppm of H<sub>2</sub>S gas, the response, response and recovery time were noted as 34.31%, 209 s and 900 s, respectively. The sensor is said to have dynamic properties and the ability to restore resistance and exhibit great uniformity. The SnO<sub>2</sub>-rGO exhibits a dynamic reversible cycle towards H<sub>2</sub>S gas.

Mirmotallebi et al. [164] showed Modified Hummer's method was used for the synthesis of graphene oxide. Copper oxide powder and ascorbic acid were mixed in a solution and drop-casted on the substrate with gold interdigitated electrodes. For sensing measurements, different operating temperatures between room temperature and 150 °C were taken into consideration. At 10 ppm of H<sub>2</sub>S at room temperature, it was discovered that injecting H<sub>2</sub>S gas into the chamber resistance increases, but when it is exposed to air, it does not recover completely. At the same time, complete recovery was found when the temperature increased from RT to 150 °C. GCu-3 has a linear sensitivity of around 3.2% per ppm of H<sub>2</sub>S gas in the air with concentrations ranging from 2.5 to 10 ppm, and its gas sensing response to 10 ppm of H<sub>2</sub>S gas is about 30% at room temperature. The response time decreases from 83 s at room temperature to 16 s at 150 °C as the temperature increases due to the enhanced surface reaction rate. Investigations on gas detection in the presence of humidity were conducted for RH values ranging from 3 to 80%. Zhou et al. [165] used a hydrothermal method to synthesise the rGO/Cu<sub>2</sub>O nanomaterials, and the lithography technique was employed for Ti, and Au layers were fabricated on a SiO<sub>2</sub>/Si substrate. When the H<sub>2</sub>S gas is exposed to 1ppm at 25 °C, only partial recovery is found after purification. But when the temperature increased to 40 °C, complete recovery was achieved. The response reached only 20% at 1 ppm of H<sub>2</sub>S gas and shows that continuous increase with higher concentration. When the sensor was exposed to other gases, it obtained a higher response toward H<sub>2</sub>S gas. The prepared rGO/Cu<sub>2</sub>O has complete recovery, selectivity, long-term stability and repeatability.

### d. Ammonia sensors

Jeevitha et al. [166] demonstrated that rGO/WO<sub>3</sub> nanocomposites with porosity were synthesized using the ultrasonication technique. The synthesized materials were ultrasonically treated, and the spin coating was used to deposit thin films of these materials. In this, it is mentioned about NH<sub>3</sub> gas detection at room temperature using rGO/WO<sub>3</sub> nanocomposites. The detection of various concentrations 10–100 ppm using rGO/WO<sub>3</sub> nanocomposite was measured at 35 °C. As the amount of rGO content increased, an increase in resistance was observed. The response and recovery time of the sensor were 18 s and

24 s, respectively. It was observed that as the  $\text{NH}_3$  gas concentration increases, it leads to a decrease in response time. The response values for  $\text{WO}_3$  and 1%, 5%, and 10%  $\text{rGO}/\text{WO}_3$  to 100 ppm  $\text{NH}_3$  gas are 10.5, 14.53, 16.0, and 0.60, respectively. In comparison with the other two percentages of  $\text{rGO}/\text{WO}_3$  nanocomposites and pure  $\text{WO}_3$ , the 5%  $\text{rGO}/\text{WO}_3$  nanocomposite exhibits good selectivity and the maximum response to  $\text{NH}_3$  gas. Andre et al. [167] used the electrospinning process and calcination treatment, and the NFI-rGO was produced. Conventional photolithography was used to fabricate the gold IDEs. At room temperature, gas sensing measurements were performed. By exposing the sensor to a range of  $\text{NH}_3$  gas concentrations (1–60 ppm), the sensor's gas detection abilities were investigated. The sensors were tested at a concentration of 15 ppm  $\text{NH}_3$  gas. It was found that NFI-rGO was 10 times greater than NFI and rGO had the highest performance. When NFI-rGO was exposed to  $\text{NH}_3$  gas at 60 ppm, response and recovery times were 17 s and 214 s. When the sensor was exposed to 45 ppm of  $\text{NH}_3$  gas for four cycles, the results had good repeatability and similar responses for all the cycles.

Sakthivel et al. [168] used modified Hummer's method for GO synthesis. The hydrothermal method was used for the synthesis of CuO nanoparticles. Both the reduction of GO to rGO development of CuO nanoparticles on the rGO nanosheets can be obtained simultaneously. The CuO-rGO nanocomposite sensors that were developed demonstrated better sensing response to  $\text{NH}_3$  gas at both room temperature and high temperatures. The rGO-CuO nanocomposite sensor exhibited an enhanced sensor response of 13 at 30 °C, and it had a sensor response of 30 at 300 °C. The sensor response increase as the concentration of the gas increases and decreases with an increase in temperature. The response of GC200 nanocomposite at 150 °C was 9 for 6.5 ppm and 30 for 600 ppm. The sensor response and recovery time were 162 and 40 s at 150 °C for 6.5 ppm. It was suggested that the sensors could be employed for long-term utility. A fast response time to 6.5 ppm in the 40 s and to 600 ppm in 16 s of  $\text{NH}_3$  gas at room temperature was shown by the GC200 sensor. At 150 °C, it was discovered that the sensor responded even more quickly. Response times at RT were reported for 6.5 ppm to be 16 s and for 600 ppm is 12 s. It was observed that the recovery time increased as the  $\text{NH}_3$  gas concentration increased. When the sensor was exposed to different gases, it showed that the maximum response was towards  $\text{NH}_3$  gas and lower responses towards other gases.

Wang et al. [169] used the hydrothermal technique to synthesize the  $\text{rGO}/\text{WS}_2$  composites where the mixture was heated at 180 °C for 16 h. The substrate was heated chip, alumina plate and IDE were placed one above the other. The sensor was exposed to different concentrations of 10–50 ppm of  $\text{NH}_3$  gas at room temperature. The  $\text{rGO}/\text{WS}_2$ -based sensor fabricated reveals a better sensing performance regarding the sensitivity and response/recovery speeds. The response and recovery time for the  $\text{rGO}/\text{WS}_2$  at 33.5 °C to 10 ppm are the 60 s and 300 s, respectively, with 20% relative humidity. From room temperature to 100 °C, the response of the  $\text{rGO}/\text{WS}_2$  sensor to 10 ppm  $\text{NH}_3$  dropped down. It was observed that when working temperatures increase,  $\text{NH}_3$  adsorption efficiency decreases. When the sensor was exposed to different gases, it showed excellent selectivity towards  $\text{NH}_3$  gas and no response towards  $\text{NO}_2$  gas. Pasha et al. [170] used the sonication method for the preparation of rGO, and by spin coating technique, thin films were fabricated. The gas sensor device has been developed using the ITO-coated glass substrate. To examine the sensing behaviour of pure and rGO-doped PEDOT-PSS organic thin films were exposed to different test gases. When the sensor was exposed to  $\text{NH}_3$  gas, maximum changes in resistance occurred when compared with other gases. Response and recovery times of 10 wt.% rGO-doped PEDOT-PSS thin films on exposure to  $\text{NH}_3$  gas were 1.05 min and 2.84 min, respectively. In comparison to other test gases such as carbon monoxide, nitrogen, and  $\text{NO}_2$  gas, the sensor device fabricated using rGO-doped PEDOT-PSS thin films showed improved sensitivity (>87%) with quick response and recovery times. The gas sensitivity increased due to the addition of more rGO in the thin films. The synthesized thin film selectivity studies showed that the developed sensor has a better selection toward  $\text{NH}_3$  gas detection at room temperature.

### e. Ethanol sensors

Meng et al. [171] showed that nanostructures of GO and g-C<sub>3</sub>N<sub>4</sub> were combined by an electrostatic self-assembly method with ultrasonic dispersion. GO was completely reduced to rGO by a hydrothermal process at 100 °C for 6 h that coated ZnO nanoparticles on GO/g-C<sub>3</sub>N<sub>4</sub>. The responses of the ZnO/rGO/g-C<sub>3</sub>N<sub>4</sub> sensor have been examined at various operating temperatures ranging from 250 to 350 °C to determine the best operating temperature for developed sensors. The operating temperature of the sensors has a considerable impact on their responses. The responses to C<sub>2</sub>H<sub>5</sub>OH vapour were noticeably improved in the ZnO/rGO/g-C<sub>3</sub>N<sub>4</sub> nanomaterials when compared to pure ZnO and ZnO/rGO. The ternary nanocomposites responded to maximum response to 100 ppm C<sub>2</sub>H<sub>5</sub>OH gas at 300 °C of 178. The response and recovery time for the ZnO/rGO/g-C<sub>3</sub>N<sub>4</sub> at 300 °C to 100 ppm are 76 s and 6 s, respectively. ZnO/rGO/g-C<sub>3</sub>N<sub>4</sub> nanocomposites were discovered to have enhanced response performance and selective detection for C<sub>2</sub>H<sub>5</sub>OH gas.

Li et al. [172] reveal that ZTO NPs were added to the surface of an rGO nanosheet using a simple solvothermal technique at 160 °C for 24 h and annealing thereafter. The prepared sample is then coated on a ceramic substrate for gas sensing. To determine the ideal working temperature, the responses of the developed sensors to 100 ppm C<sub>2</sub>H<sub>5</sub>OH gas were evaluated at various temperatures from 225 to 300 °C. The maximum responses for the sensors relying on pure ZTO, 4ZTO/rGO, 8ZTO/rGO, and 40ZTO/rGO at 275 °C are 6, 22, 36, and 24, respectively. The ideal operating temperature for the sensor is therefore considered to be 275 °C. The 8ZTO/rGO sensor has the highest response rate of the three composite sensors. The response of the 8ZTO/rGO sensor at 275 °C to 100 ppm is 78. In spite of having a greater response, the 8ZTO/rGO sensor has improved selectivity, quick response and recovery time and strong linearity throughout a broad range of C<sub>2</sub>H<sub>5</sub>OH gas concentrations. Thu et al. [173] used modified Hummer's method to synthesize GO from low-cost graphite powder, and it was described as an easy and efficient chemical process with a high yield. The hydrothermal method was used to prepare the Fe<sub>3</sub>O<sub>4</sub>/rGO nanocomposites. With various reduced gases (C<sub>2</sub>H<sub>5</sub>OH, CO, H<sub>2</sub> and NH<sub>3</sub>), the α-Fe<sub>2</sub>O<sub>3</sub> nanoporous network's gas-sensing capability was examined. The sensor's C<sub>2</sub>H<sub>5</sub>OH gas-sensing capabilities were examined between 350 and 450 °C. The optimum working temperature was found to be 400 °C. The response of C<sub>2</sub>H<sub>5</sub>OH gas to 100 ppm was 9.5, whereas the cross-gas responses of other gases such as NH<sub>3</sub>, H<sub>2</sub>, and CO gases were all less than 2.0. The response and recovery times of these sensors at 400 °C to 100 ppm were 3 s and 150 s, respectively. As per the gas-sensing characteristics, the Fe<sub>2</sub>O<sub>3</sub> porous network showed good sensitivity, amazing selectivity, and great stability as a C<sub>2</sub>H<sub>5</sub>OH gas sensor.

## 4. Current Challenges of the Graphene-Based Gas Sensors

Different forms of graphene materials have been considered as per their electrochemical properties. Since pure graphene does not have a bandgap, it has been doped with other ions to increase their reactivity with the gaseous molecules. The presence of dopants increases the current as a result of the presence of free electrons. In other cases, graphene has been mixed with metallic nanomaterials and metal oxides to form composites whose conductance would change with respect to the concentration of the gases. The presence of noble metals enhances the change in the signals when the sensors react with the gases. The adsorption of the gaseous absorbents leads to the contribution of holes or electrons to graphene via weak hybridization to its surface. The presence of electron-donating gases such as NH<sub>3</sub> decreases the overall conductance, while electron-withdrawing gases such as NO<sub>2</sub> increase the resultant conductance of the prototypes [174,175]. The formation of nanocomposites with polymers induces porous microstructures to accelerate the diffusion of gaseous molecules into the sensing layers. The presence of water molecules on the sensing surface of these graphene sensors also contributes to the overall response. A significant amount of work, as shown above, has been performed on the development of graphene-based sensors and deploying them for gas-sensing applications. Table 1 shows a comparative study of the examples explained in the preceding sections. The comparison

is made based on the pivotal electrochemical gas-sensing parameters such as sensitivity, operating range, response and recovery times and operating temperature of the prototypes. It is seen that the variation in the processed materials varies the overall performances of the prototypes. In addition to the detection of the five gases to ppm and sub-ppm levels, the sensors have also been able to detect multiple gases. Although the performances of the sensors are enhanced at elevated temperatures, their efficiency in terms of sensitivity in a real-time environment is still an issue.

**Table 1.** Comparison of the performances of different graphene-based gas sensors.

Target Gas	Processed Materials	Sensitivity (Maximum)	Operating Range (ppm)	Response Time (s)	Recovery Time (s)	Operating Temp. (°C)	Ref.
CO <sub>2</sub>	Graphene nanosheets, PDMS	0.17%/ppm	10–100	8	10	Room temp.	[99]
	GQDs	50%	100, 300, 500	106	150	Room temp.	[140]
	rGO	50%	1000–7000	10, 60	-	Room temp.	[154]
NO <sub>2</sub>	Graphene nanosheets, Cu <sub>2</sub> O nanowires	0.66	0.05	279	1239	Room temp.	[100]
	GQDs, PbS	125	1–150	7	22	Room temp.	[141]
	rGO, ZnO	5.4	1, 2, 5	-	900–1800	250	[158]
H <sub>2</sub> S	Graphene nanosheets, Fe <sub>2</sub> O <sub>3</sub> , VAFe, HAFe	33.7	23	0.5	30	100–300	[107]
	NH <sub>2</sub> -GQDs, TiO <sub>2</sub>	26.62	0–55	68	77	Room temp.	[176]
	rGO, SnO <sub>2</sub>	20.87%	100	209	900	25–125	[163]
NH <sub>3</sub>	Graphene nanosheets, PANI	930%	20–100	31	500	25–100	[108]
	N-GQDs, PEDOT: PSS	116.38%	1000–1500	462	600	Room temp.	[145]
	In <sub>2</sub> O <sub>3</sub> , rGO	90%	1–60	17	214	Room temp.	[167]
C <sub>2</sub> H <sub>5</sub> OH	Graphene nanosheets, ZnO NWs,	26	1–20	-	-	125, 200	[112]
	GQDs, ZnO NRs	90%	500	-	-	Room temp.	[151]
	α-Fe <sub>3</sub> O <sub>4</sub> , rGO	9.5	10–1000	3	150	350–450	[173]

Although a lot of work has been conducted on the fabrication and implementation of graphene-based gas sensors, there are still some bottlenecks remaining in the current scenario. Quantification of the gas sensors formed in the controlled environment needs to be performed to detect their capability in terms of robustness and longevity. From the fabrication point of view, the synthesis process of graphene is still an issue. The currently used processes, such as CVD and mechanical exfoliation, are not suitable for mass production due to the requirement of highly expensive equipment. The CVD process also generates toxic gaseous by-products, thus increasing the requirement of health and safety protocols. Additionally, the various fabrication processes, as mentioned in the paper, subsequently generate graphene with varied electromechanical properties. Thus, it is difficult to standardize the fabrication process that can be used to develop high-quality graphene. Although the use of graphite to develop graphene has been one of the popular ways, some of the demerits associated with graphite-like low current density, high contact resistance and low oxidation temperature decrease its quality as a pre-cursor material [177]. The use of printing techniques for forming these sensors should be further studied to optimize certain parameters e.g., surface tension and viscosity of the conductive inks. The conjugation of graphene with other nanomaterials to form the nanocomposites is another area that needs to be worked on. Since the customization of the bandgap of graphene is necessary for tailoring the sensitivity of the gas-sensing prototypes, the techniques used to develop the covalent bonding between the nanomaterials and graphene need to be studied and worked upon. The hydrophilic nature of rGO is another issue that needs to be resolved

during the formation of the sensors. The consistency in the sensitivity of these sensors is another area that needs to be resolved. Since the sensitivity of prototypes degrades with prolonged use, consistency is required to reduce the frequency of replacement of the sensors during their real-time application. Dynamic thresholding should be conducted on the sensitivity to realize their performances in terms of extensive use and longevity. The researchers should also work to enhance the quality of the sensors in terms of their selective nature towards the targeted gases. Even though the above-mentioned prototypes have been capable of detecting individual gases at wide concentrations, the presence of multiple gases in real-time scenarios is still something to be dealt with. The interference of the gases and other volatile organic compounds during the detection process would also affect the accuracy and sensitivity of the prototypes. The combination of two nanomaterials to increase the number of detected gases using a single prototype can be a probable option. The formation of an array of gas sensors in a single system can be conducted to use for targeting common gases. While some of the prototypes operate in the presence of a selective layer for adsorption purposes, their reusability is another bottleneck that needs to be addressed. This would increase the overall cost of operation as the replacement of sensors in particular accessed locations and harsh environments would need expertise and the expensive equipment. As the sensors are used for a long period of time to test their longevity, the stability and reproducibility of the results are two factors that need to be worked upon. The fluctuation of results for dangerous industrial gases can give false alarms leading to disastrous consequences. The reproducibility of the results would also assist in determining the quality of service (QoS) of the prototypes when they are considered for commercial purposes. The fabrication techniques for the deposition of the selective layer should be further researched to determine the exact position of the added selective nanoparticles or colloidal layer. A proper comparison should be made on the capability of deposition techniques in terms of the nanoparticles, thickness, strength, and gases detected with respect to each nanomaterial. The degree of bonding between the selective layer with the electrodes can determine the capacity of the prototypes to operate for a long time under extreme conditions. Better material characterization of the selective layer can assist in studying the functionalization that can be performed to increase their detecting capabilities. As the conservation of energy is pivotal in the current world, the sensing systems should be designed in such a way that the input power to a single prototype is negligible. From an academic point of view, further studies should be carried out on the graphene-based gas sensors that have the same design and dimension but are formed with different allotropes. Further work should be conducted on the selective materials used on top of the electrodes to increase the selectivity towards the targeted gases. The operating range and LOD should be widened for these graphene-based sensors to singularize the use of the same prototype for both domestic and industrial applications. Further research should be conducted on the capability of these sensors to detect harmful gases whose presence in the atmosphere in minor concentrations can create disastrous consequences. Some of the above-mentioned examples should be integrated with wireless communication to detect their responses as wearable sensing systems. The multifunctional nature of these graphene-based sensors should be further highlighted to induce both electrochemical and strain-sensing nature.

## 5. Conclusions

The paper showcases the use of graphene sensors for gas-sensing applications. Different physical forms of graphene structures have been integrated with polymers to form flexible and rigid prototypes that can detect gases at different concentrations. Some of the advantages of these graphene-based sensors include their high sensitivity, operating range and LOD. The operation of these sensors has been carried out both in the room and at elevated temperatures. Although the proof-of-concept of these gas sensors has been shown in this paper, further work needs to be performed to form fully operating gas-sensing systems that can operate in real-time conditions. The amalgamation of these sensing systems with wireless communication would also help the prototypes to be operated in

domestic and industrial scenarios at specified intervals. The state-of-the-art requirement to develop better versions of gas sensors in terms of their dynamic characteristics needs to be carried out with collaborative work between the academic and industrial institutions. Structured modifications to the fabrication processes of graphene and gas sensors would be highly beneficial in their value-added products. The exceptional attributes of graphene have allowed these gas sensors to be merged with different activities of human life, thus improving the overall quality of life.

**Author Contributions:** Conceptualization, A.C., A.N., Methodology, A.C., A.N., M.E.E.A., N.A., Validation, A.N., M.E.A., Investigation, A.C., S.N., A.N., M.E.E.A., N.A., resources, A.C., A.N., writing—original draft preparation, A.C., A.N., M.E.E.A., N.A.; writing—review and editing, A.C., S.N., A.N., M.E.E.A., N.A.; visualization, A.N., M.E.A.; supervision, M.E.A. All authors have read and agreed to the published version of the manuscript.

**Funding:** This research received no external funding.

**Institutional Review Board Statement:** Not applicable.

**Informed Consent Statement:** Not applicable.

**Acknowledgments:** Funded by the German Research Foundation (DFG, Deutsche Forschungsgemeinschaft) as part of Germany's Excellence Strategy—EXC 2050/1—Project ID 390696704—Cluster of Excellence “Centre for Tactile Internet with Human-in-the-Loop” (CeTI) of Technische Universität Dresden.

**Conflicts of Interest:** The authors declare no conflict of interest.

## References

1. Novoselov, K.S.; Colombo, L.; Gellert, P.; Schwab, M.; Kim, K. A roadmap for graphene. *Nature* **2012**, *490*, 192–200. [[CrossRef](#)] [[PubMed](#)]
2. Geim, A.K. Graphene: Status and prospects. *Science* **2009**, *324*, 1530–1534. [[CrossRef](#)]
3. Geim, A.K.; Novoselov, K.S. The rise of graphene. In *Nanoscience and Technology: A Collection of Reviews from Nature Journals*; World Scientific: Singapore, 2010; pp. 11–19.
4. Kurian, A.S.; Mohan, V.B.; Souri, H.; Leng, J.; Bhattacharyya, D. Multifunctional flexible and stretchable graphite-silicone rubber composites. *J. Mater. Res. Technol.* **2020**, *9*, 15621–15630. [[CrossRef](#)]
5. Nag, A.; Alahi, M.E.E.; Feng, S.; Mukhopadhyay, S.C. IoT-based sensing system for phosphate detection using Graphite/PDMS sensors. *Sens. Actuators A Phys.* **2019**, *286*, 43–50. [[CrossRef](#)]
6. Zhang, M.; Wang, C.; Wang, Q.; Jian, M.; Zhang, Y. Sheath–core graphite/silk fiber made by dry-meyer-rod-coating for wearable strain sensors. *ACS Appl. Mater. Interfaces* **2016**, *8*, 20894–20899. [[CrossRef](#)] [[PubMed](#)]
7. Lau, C.N.; Bao, W.; Velasco, J., Jr. Properties of suspended graphene membranes. *Mater. Today* **2012**, *15*, 238–245. [[CrossRef](#)]
8. Nag, A.; Alahi, M.E.E.; Mukhopadhyay, S.C. Recent progress in the fabrication of graphene fibers and their composites for applications of monitoring human activities. *Appl. Mater. Today* **2021**, *22*, 100953. [[CrossRef](#)]
9. Dalal, M.H.; Lee, C.-Y.; Wallace, G.G. Cathodic exfoliation of graphite into graphene nanoplatelets in aqueous solution of alkali metal salts. *J. Mater. Sci.* **2021**, *56*, 3612–3622. [[CrossRef](#)]
10. Shirhatti, V.; Nuthalapati, S.; Kedambaimoole, V.; Kumar, S.; Nayak, M.M.; Rajanna, K. Multifunctional graphene sensor ensemble as a smart biomonitoring fashion accessory. *ACS Sens.* **2021**, *6*, 4325–4337. [[CrossRef](#)]
11. Yu, H.; Guo, W.; Lu, X.; Xu, H.; Yang, Q.; Tan, J.; Zhang, W. Reduced graphene oxide nanocomposite based electrochemical biosensors for monitoring foodborne pathogenic bacteria: A review. *Food Control* **2021**, *127*, 108117. [[CrossRef](#)]
12. Shao, Y.; Wang, J.; Wu, H.; Liu, J.; Aksay, I.A.; Lin, Y. Graphene based electrochemical sensors and biosensors: A review. *Electroanal. Int. J. Devoted Fundam. Pract. Asp. Electroanal.* **2010**, *22*, 1027–1036. [[CrossRef](#)]
13. Gao, J.; He, S.; Nag, A.; Wong, J.W.C. A Review of the Use of Carbon Nanotubes and Graphene-Based Sensors for the Detection of Aflatoxin M1 Compounds in Milk. *Sensors* **2021**, *21*, 3602. [[CrossRef](#)] [[PubMed](#)]
14. Hu, Q.; Nag, A.; Xu, Y.; Han, T.; Zhang, L. Use of graphene-based fabric sensors for monitoring human activities. *Sens. Actuators A Phys.* **2021**, *332*, 113172. [[CrossRef](#)]
15. Mehmood, A.; Mubarak, N.; Khalid, M.; Walvekar, R.; Abdullah, E.; Siddiqui, M.; Baloch, H.A.; Nizamuddin, S.; Mazari, S. Graphene based nanomaterials for strain sensor application—A review. *J. Environ. Chem. Eng.* **2020**, *8*, 103743. [[CrossRef](#)]
16. Wang, T.; Ouyang, Z.; Wang, F.; Liu, Y. A review on graphene strain sensors based on fiber assemblies. *SN Appl. Sci.* **2020**, *2*, 862. [[CrossRef](#)]
17. Nuthalapati, S.; Shirhatti, V.; Kedambaimoole, V.; Takao, H.; Nayak, M.; Rajanna, K. Highly sensitive flexible strain and temperature sensors using solution processed graphene palladium nanocomposite. *Sens. Actuators A Phys.* **2022**, *334*, 113314. [[CrossRef](#)]

18. Vasseghian, Y.; Dragoi, E.-N.; Moradi, M.; Khaneghah, A.M. A review on graphene-based electrochemical sensor for mycotoxins detection. *Food Chem. Toxicol.* **2021**, *148*, 111931.
19. Fanizza, C.; Stefanelli, M.; Risuglia, A.; Bruni, E.; Ietto, F.; Incoronato, F.; Marra, F.; Preziosi, A.; Mancini, P.; Sarto, M.S. In Vitro and In Vivo Biocompatibility Studies on Engineered Fabric with Graphene Nanoplatelets. *Nanomaterials* **2022**, *12*, 1405. [[CrossRef](#)]
20. Jia, G.; Zheng, A.; Wang, X.; Zhang, L.; Li, L.; Li, C.; Zhang, Y.; Cao, L. Flexible, biocompatible and highly conductive MXene-graphene oxide film for smart actuator and humidity sensor. *Sens. Actuators B Chem.* **2021**, *346*, 130507. [[CrossRef](#)]
21. Veerakumar, P.; Sangili, A.; Chen, S.-M.; Vinothkumar, V.; Balu, S.; Hung, S.-T.; Lin, K.-C. Zinc and Sulfur Codoped Iron Oxide Nanocubes Anchored on Carbon Nanotubes for the Detection of Antitubercular Drug Isoniazid. *ACS Appl. Nano Mater.* **2021**, *4*, 4562–4575. [[CrossRef](#)]
22. Kao, H.-L.; Cho, C.-L.; Chang, L.-C.; Chen, C.-B.; Chung, W.-H.; Tsai, Y.-C. A Fully Inkjet-Printed Strain Sensor Based on Carbon Nanotubes. *Coatings* **2020**, *10*, 792. [[CrossRef](#)]
23. Daňová, R.; Olejník, R.; Slobodian, P.; Matyas, J. The Piezoresistive Highly Elastic Sensor Based on Carbon Nanotubes for the Detection of Breath. *Polymers* **2020**, *12*, 713. [[CrossRef](#)] [[PubMed](#)]
24. Kausar, A. Poly (methyl methacrylate) nanocomposite reinforced with graphene, graphene oxide, and graphite: A review. *Polym.-Plast. Technol. Mater.* **2019**, *58*, 821–842. [[CrossRef](#)]
25. Huang, Y.; Zeng, X.; Wang, W.; Guo, X.; Hao, C.; Pan, W.; Liu, P.; Liu, C.; Ma, Y.; Zhang, Y. High-resolution flexible temperature sensor based graphite-filled polyethylene oxide and polyvinylidene fluoride composites for body temperature monitoring. *Sens. Actuators A Phys.* **2018**, *278*, 1–10. [[CrossRef](#)]
26. Thompson, B.C.; Murray, E.; Wallace, G.G. Graphite oxide to graphene. Biomaterials to bionics. *Adv. Mater.* **2015**, *27*, 7563–7582. [[CrossRef](#)] [[PubMed](#)]
27. Akinwande, D.; Huyghebaert, C.; Wang, C.-H.; Serna, M.I.; Goossens, S.; Li, L.-J.; Wong, H.-S.P.; Koppens, F.H. Graphene and two-dimensional materials for silicon technology. *Nature* **2019**, *573*, 507–518. [[CrossRef](#)]
28. Zaky, Z.A.; Aly, A.H. Gyroidal graphene/porous silicon array for exciting optical Tamm state as optical sensor. *Sci. Rep.* **2021**, *11*, 19389. [[CrossRef](#)]
29. He, S.; Zhang, Y.; Gao, J.; Nag, A.; Rahaman, A. Integration of Different Graphene Nanostructures with PDMS to Form Wearable Sensors. *Nanomaterials* **2022**, *12*, 950. [[CrossRef](#)]
30. Nag, A.; Simorangkir, R.B.; Valentin, E.; Björninen, T.; Ukkonen, L.; Hashmi, R.M.; Mukhopadhyay, S.C. A transparent strain sensor based on PDMS-embedded conductive fabric for wearable sensing applications. *IEEE Access* **2018**, *6*, 71020–71027. [[CrossRef](#)]
31. Nag, A.; Mukhopadhyay, S.C.; Kosel, J. Tactile sensing from laser-ablated metallized PET films. *IEEE Sens. J.* **2016**, *17*, 7–13. [[CrossRef](#)]
32. Emamian, S.; Narakathu, B.B.; Chlahawi, A.A.; Bazuin, B.J.; Atashbar, M.Z. Screen printing of flexible piezoelectric based device on polyethylene terephthalate (PET) and paper for touch and force sensing applications. *Sens. Actuators A Phys.* **2017**, *263*, 639–647. [[CrossRef](#)]
33. Han, T.; Nag, A.; Afsarimanesh, N.; Akhter, F.; Liu, H.; Sapra, S.; Mukhopadhyay, S.; Xu, Y. Gold/Polyimide-Based Resistive Strain Sensors. *Electronics* **2019**, *8*, 565. [[CrossRef](#)]
34. Nag, A.; Mukhopadhyay, S.C. Fabrication and implementation of printed sensors for taste sensing applications. *Sens. Actuators A Phys.* **2018**, *269*, 53–61. [[CrossRef](#)]
35. Geleta, G.S.; Zhao, Z.; Wang, Z. A novel reduced graphene oxide/molybdenum disulfide/polyaniline nanocomposite-based electrochemical aptasensor for detection of aflatoxin B 1. *Analyst* **2018**, *143*, 1644–1649. [[CrossRef](#)] [[PubMed](#)]
36. Ünsal, Ö.F.; Altın, Y.; Çelik Bedeloğlu, A. Poly (vinylidene fluoride) nanofiber-based piezoelectric nanogenerators using reduced graphene oxide/polyaniline. *J. Appl. Polym. Sci.* **2020**, *137*, 48517. [[CrossRef](#)]
37. Lee, S.; Eom, T.; Kim, M.-K.; Yang, S.-G.; Shim, B.S. Durable soft neural micro-electrode coating by an electrochemical synthesis of PEDOT: PSS/graphene oxide composites. *Electrochim. Acta* **2019**, *313*, 79–90. [[CrossRef](#)]
38. Vuorinen, T.; Niittynen, J.; Kankkunen, T.; Kraft, T.M.; Mäntysalo, M. Inkjet-printed graphene/PEDOT: PSS temperature sensors on a skin-conformable polyurethane substrate. *Sci. Rep.* **2016**, *6*, 35289. [[CrossRef](#)]
39. Dhinakaran, V.; Stalin, B.; Sai, M.S.; Vairamuthu, J.; Marichamy, S. Recent developments of graphene composites for energy storage devices. *Mater. Today Proc.* **2021**, *45*, 1779–1782. [[CrossRef](#)]
40. Lakra, R.; Kumar, R.; Sahoo, P.K.; Thatoi, D.; Soam, A. A mini-review: Graphene based composites for supercapacitor application. *Inorg. Chem. Commun.* **2021**, *133*, 108929. [[CrossRef](#)]
41. Kaminiaris, M.D.; Mavrikou, S.; Georgiadou, M.; Paivana, G.; Tsitsigiannis, D.I.; Kintzios, S. An Impedance Based Electrochemical Immunosensor for Aflatoxin B1 Monitoring in Pistachio Matrices. *Chemosensors* **2020**, *8*, 121. [[CrossRef](#)]
42. Jahangiri–Dehaghani, F.; Zare, H.R.; Shekari, Z. Measurement of aflatoxin M1 in powder and pasteurized milk samples by using a label-free electrochemical aptasensor based on platinum nanoparticles loaded on Fe-based metal-organic frameworks. *Food Chem.* **2020**, *310*, 125820. [[CrossRef](#)]
43. Jeong, S.-Y.; Ma, Y.-W.; Lee, J.-U.; Je, G.-J.; Shin, B.-S. Flexible and Highly Sensitive Strain Sensor Based on Laser-Induced Graphene Pattern Fabricated by 355 nm Pulsed Laser. *Sensors* **2019**, *19*, 4867. [[CrossRef](#)]
44. Zhang, F.; Wu, S.; Peng, S.; Sha, Z.; Wang, C.H. Synergism of binary carbon nanofibres and graphene nanoplates in improving sensitivity and stability of stretchable strain sensors. *Compos. Sci. Technol.* **2019**, *172*, 7–16. [[CrossRef](#)]



45. Huang, T.; He, P.; Wang, R.; Yang, S.; Sun, J.; Xie, X.; Ding, G. Porous fibers composed of polymer nanoball decorated graphene for wearable and highly sensitive strain sensors. *Adv. Funct. Mater.* **2019**, *29*, 1903732. [[CrossRef](#)]
46. Nuthalapati, S.; Kedambaimoole, V.; Shirhatti, V.; Kumar, S.; Takao, H.; Nayak, M.; Rajanna, K. Flexible strain sensor with high sensitivity, fast response, and good sensing range for wearable applications. *Nanotechnology* **2021**, *32*, 505506. [[CrossRef](#)] [[PubMed](#)]
47. Muthumariyappan, A.; Rajaji, U.; Chen, S.-M.; Baskaran, N.; Chen, T.-W.; Ramalingam, R.J. Sonochemical synthesis of perovskite-type barium titanate nanoparticles decorated on reduced graphene oxide nanosheets as an effective electrode material for the rapid determination of ractopamine in meat samples. *Ultrason. Sonochemistry* **2019**, *56*, 318–326. [[CrossRef](#)] [[PubMed](#)]
48. Shamsaei, E.; de Souza, F.B.; Yao, X.; Benhelal, E.; Akbari, A.; Duan, W. Graphene-based nanosheets for stronger and more durable concrete: A review. *Constr. Build. Mater.* **2018**, *183*, 642–660. [[CrossRef](#)]
49. Huang, Q.; Lin, X.; Tong, L.; Tong, Q.-X. Graphene Quantum Dots/Multiwalled Carbon Nanotubes Composite-Based Electrochemical Sensor for Detecting Dopamine Release from Living Cells. *ACS Sustain. Chem. Eng.* **2020**, *8*, 1644–1650. [[CrossRef](#)]
50. Mansuriya, B.D.; Altintas, Z. Applications of graphene quantum dots in biomedical sensors. *Sensors* **2020**, *20*, 1072. [[CrossRef](#)]
51. Baloda, S.; Ansari, Z.A.; Singh, S.; Gupta, N. Development and Analysis of Graphene Nanoplatelets (GNP) Based Flexible Strain Sensor for Health Monitoring Applications. *IEEE Sens. J.* **2020**, *20*, 13302–13309. [[CrossRef](#)]
52. Gouda, K.; Bhowmik, S.; Das, B. Thermomechanical behavior of graphene nanoplatelets and bamboo micro filler incorporated epoxy hybrid composites. *Mater. Res. Express* **2020**, *7*, 015328. [[CrossRef](#)]
53. Nuthalapati, S.; Shirhatti, V.; Kedambaimoole, V.; Neella, N.; Nayak, M.; Rajanna, K.; Takao, H. Highly sensitive, scalable reduced graphene oxide with palladium nano-composite as strain sensor. *Nanotechnology* **2019**, *31*, 035501. [[CrossRef](#)] [[PubMed](#)]
54. Zheng, C.; Zhang, C.; Zhang, K.; Zhang, J.; Jin, L.; Asiri, A.M.; Alamry, K.A.; He, L.; Chu, X. Growth of ZnFe<sub>2</sub>O<sub>4</sub> nanosheets on reduced graphene oxide with enhanced ethanol sensing properties. *Sens. Actuators B Chem.* **2021**, *330*, 129280. [[CrossRef](#)]
55. Sharma, A.; Morisada, Y.; Fujii, H. Bending induced mechanical exfoliation of graphene interlayers in a through thickness Al-GNP functionally graded composite fabricated via novel single-step FSP approach. *Carbon* **2022**, *186*, 475–491. [[CrossRef](#)]
56. Ma, Y.; Bai, D.; Hu, X.; Ren, N.; Gao, W.; Chen, S.; Chen, H.; Lu, Y.; Li, J.; Bai, Y. Robust and antibacterial polymer/mechanically exfoliated graphene nanocomposite fibers for biomedical applications. *ACS Appl. Mater. Interfaces* **2018**, *10*, 3002–3010. [[CrossRef](#)]
57. Li, G.; Zhang, Y.-Y.; Guo, H.; Huang, L.; Lu, H.; Lin, X.; Wang, Y.-L.; Du, S.; Gao, H.-J. Epitaxial growth and physical properties of 2D materials beyond graphene: From monatomic materials to binary compounds. *Chem. Soc. Rev.* **2018**, *47*, 6073–6100. [[CrossRef](#)]
58. Shao, Y.; Liu, Z.-L.; Cheng, C.; Wu, X.; Liu, H.; Liu, C.; Wang, J.-O.; Zhu, S.-Y.; Wang, Y.-Q.; Shi, D.-X. Epitaxial growth of flat antimonene monolayer: A new honeycomb analogue of graphene. *Nano Lett.* **2018**, *18*, 2133–2139. [[CrossRef](#)]
59. Zhang, T.; Liao, Z.; Sandonas, L.M.; Dianat, A.; Liu, X.; Xiao, P.; Amin, I.; Gutierrez, R.; Chen, T.; Zschech, E. Polymerization driven monomer passage through monolayer chemical vapour deposition graphene. *Nat. Commun.* **2018**, *9*, 4051. [[CrossRef](#)]
60. Saeed, M.; Alshammari, Y.; Majeed, S.A.; Al-Nasrallah, E. Chemical vapour deposition of graphene—Synthesis, characterisation, and applications: A review. *Molecules* **2020**, *25*, 3856. [[CrossRef](#)]
61. Zhang, Y.; Li, N.; Xiang, Y.; Wang, D.; Zhang, P.; Wang, Y.; Lu, S.; Xu, R.; Zhao, J. A flexible non-enzymatic glucose sensor based on copper nanoparticles anchored on laser-induced graphene. *Carbon* **2020**, *156*, 506–513. [[CrossRef](#)]
62. Huang, L.; Su, J.; Song, Y.; Ye, R. Laser-Induced Graphene: En Route to Smart Sensing. *Nano-Micro Lett.* **2020**, *12*, 157. [[CrossRef](#)] [[PubMed](#)]
63. De Silva, K.; Huang, H.-H.; Joshi, R.; Yoshimura, M. Chemical reduction of graphene oxide using green reductants. *Carbon* **2017**, *119*, 190–199. [[CrossRef](#)]
64. Chua, C.K.; Pumbera, M. Chemical reduction of graphene oxide: A synthetic chemistry viewpoint. *Chem. Soc. Rev.* **2014**, *43*, 291–312. [[CrossRef](#)]
65. Bleu, Y.; Bourquard, F.; Tite, T.; Loir, A.-S.; Maddi, C.; Donnet, C.; Garrelie, F. Review of graphene growth from a solid carbon source by pulsed laser deposition (PLD). *Front. Chem.* **2018**, *6*, 572. [[CrossRef](#)] [[PubMed](#)]
66. Boukhvalov, D.; Katsnelson, M.; Lichtenstein, A. Hydrogen on graphene: Electronic structure, total energy, structural distortions and magnetism from first-principles calculations. *Phys. Rev. B* **2008**, *77*, 035427. [[CrossRef](#)]
67. Tian, P.; Tang, L.; Teng, K.; Lau, S. Graphene quantum dots from chemistry to applications. *Mater. Today Chem.* **2018**, *10*, 221–258. [[CrossRef](#)]
68. Sang, M.; Shin, J.; Kim, K.; Yu, K.J. Electronic and thermal properties of graphene and recent advances in graphene based electronics applications. *Nanomaterials* **2019**, *9*, 374. [[CrossRef](#)]
69. Wang, W.; Zhang, Y.; Shen, C.; Chai, Y. Adsorption of CO molecules on doped graphene: A first-principles study. *Aip Adv.* **2016**, *6*, 025317. [[CrossRef](#)]
70. Li, N.; Zhen, Z.; Xu, Z.; Zhang, R.; Mu, R.; He, L. The growth of large-sized graphene domains by Faraday cage-assisted plasma enhanced chemical vapor deposition. *Appl. Surf. Sci. Adv.* **2021**, *6*, 100154. [[CrossRef](#)]
71. Thangamani, G.; Deshmukh, K.; Kovářík, T.; Nambiraj, N.; Ponnamm, D.; Sadasivuni, K.K.; Khalil, H.A.; Pasha, S.K. Graphene oxide nanocomposites based room temperature gas sensors: A review. *Chemosphere* **2021**, *280*, 130641. [[CrossRef](#)] [[PubMed](#)]
72. Shah, N.A.; Gul, M.; Abbas, M.; Amin, M. Synthesis of Metal Oxide Semiconductor Nanostructures for Gas Sensors. In *Gas Sensors*; IntechOpen: London, UK, 2019.
73. Stanford, M.G.; Yang, K.; Chyan, Y.; Kittrell, C.; Tour, J.M. Laser-induced graphene for flexible and embeddable gas sensors. *ACS Nano* **2019**, *13*, 3474–3482. [[CrossRef](#)] [[PubMed](#)]

74. Seekaew, Y.; Wongchoosuk, C. A novel graphene-based electroluminescent gas sensor for carbon dioxide detection. *Appl. Surf. Sci.* **2019**, *479*, 525–531. [[CrossRef](#)]
75. He, X.; Liu, Q.; Wang, J.; Chen, H. Wearable gas/strain sensors based on reduced graphene oxide/linen fabrics. *Front. Mater. Sci.* **2019**, *13*, 305–313. [[CrossRef](#)]
76. Ahmad, R.; Majhi, S.M.; Zhang, X.; Swager, T.M.; Salama, K.N. Recent progress and perspectives of gas sensors based on vertically oriented ZnO nanomaterials. *Adv. Colloid Interface Sci.* **2019**, *270*, 1–27. [[CrossRef](#)]
77. Zhu, J.; Cho, M.; Li, Y.; He, T.; Ahn, J.; Park, J.; Ren, T.-L.; Lee, C.; Park, I. Machine learning-enabled textile-based graphene gas sensing with energy harvesting-assisted IoT application. *Nano Energy* **2021**, *86*, 106035. [[CrossRef](#)]
78. Padvi, M.; Moholkar, A.; Prasad, S.; Prasad, N. A critical review on design and development of gas sensing materials. *Eng. Sci.* **2021**, *15*, 20–37. [[CrossRef](#)]
79. Oh, W.-C.; Liu, Y.; Sagadevan, S.; Fatema, K.N.; Biswas, M.R.U.D. Polymer bonded Graphene-LaNiSbWO<sub>4</sub> nanocomposite (G-LaNiSbWO<sub>4</sub>-PPy) for CO<sub>2</sub> sensing performance under normal temperature condition. *Inorg. Nano-Met. Chem.* **2021**, *51*, 1803–1812. [[CrossRef](#)]
80. Salih, E.; Ayesh, A.I. Pt-doped armchair graphene nanoribbon as a promising gas sensor for CO and CO<sub>2</sub>: DFT study. *Phys. E Low-Dimens. Syst. Nanostructures* **2021**, *125*, 114418. [[CrossRef](#)]
81. Tang, X.; Debliquy, M.; Lahem, D.; Yan, Y.; Raskin, J.-P. A review on functionalized graphene sensors for detection of ammonia. *Sensors* **2021**, *21*, 1443. [[CrossRef](#)]
82. Zhu, Y.; Yu, L.; Wu, D.; Lv, W.; Wang, L. A high-sensitivity graphene ammonia sensor via aerosol jet printing. *Sens. Actuators A Phys.* **2021**, *318*, 112434. [[CrossRef](#)]
83. Bibi, A.; Rubio, Y.R.M.; Xian-Lun, L.; Sathishkumar, N.; Chen, C.-Y.; Santiago, K.S.; Chen, H.-T.; Lin, Y.-F.; Yeh, J.-M. Detection of hydrogen sulfide using polyaniline incorporated with graphene oxide aerogel. *Synth. Met.* **2021**, *282*, 116934. [[CrossRef](#)]
84. Liu, L.; Jiang, Y.; Jiang, J.; Zhou, J.; Xu, Z.; Li, Y. Flexible and Transparent Silver Nanowires Integrated with a Graphene Layer-Doping PEDOT: PSS Film for Detection of Hydrogen Sulfide. *ACS Appl. Electron. Mater.* **2021**, *3*, 4579–4586. [[CrossRef](#)]
85. Xiong, S.; Zhou, J.; Wu, J.; Li, H.; Zhao, W.; He, C.; Liu, Y.; Chen, Y.; Fu, Y.; Duan, H. High performance acoustic wave nitrogen dioxide sensor with ultraviolet activated 3D porous architecture of Ag-decorated reduced graphene oxide and polypyrrole aerogel. *ACS Appl. Mater. Interfaces* **2021**, *13*, 42094–42103. [[CrossRef](#)] [[PubMed](#)]
86. Pisarkiewicz, T.; Maziarz, W.; Małolepszy, A.; Stobiński, L.; Michoń, D.A.; Szkudlarek, A.; Pisarek, M.; Kanak, J.; Rydosz, A. Nitrogen dioxide sensing using multilayer structure of reduced graphene oxide and  $\alpha$ -Fe<sub>2</sub>O<sub>3</sub>. *Sensors* **2021**, *21*, 1011. [[CrossRef](#)]
87. Rafiee, Z.; Roshan, H.; Sheikhi, M.H. Low concentration ethanol sensor based on graphene/ZnO nanowires. *Ceram. Int.* **2021**, *47*, 5311–5317. [[CrossRef](#)]
88. Dey, A. Semiconductor metal oxide gas sensors: A review. *Mater. Sci. Eng. B* **2018**, *229*, 206–217. [[CrossRef](#)]
89. Levitsky, I.A. Porous silicon structures as optical gas sensors. *Sensors* **2015**, *15*, 19968–19991. [[CrossRef](#)]
90. Balasubramani, V.; Chandraleka, S.; Rao, T.S.; Sasikumar, R.; Kuppusamy, M.; Sridhar, T. Recent advances in electrochemical impedance spectroscopy based toxic gas sensors using semiconducting metal oxides. *J. Electrochem. Soc.* **2020**, *167*, 037572. [[CrossRef](#)]
91. Zhai, Z.; Zhang, X.; Hao, X.; Niu, B.; Li, C. Metal–Organic Frameworks Materials for Capacitive Gas Sensors. *Adv. Mater. Technol.* **2021**, *6*, 2100127. [[CrossRef](#)]
92. Cho, S.H.; Suh, J.M.; Eom, T.H.; Kim, T.; Jang, H.W. Colorimetric sensors for toxic and hazardous gas detection: A review. *Electron. Mater. Lett.* **2021**, *17*, 1–17. [[CrossRef](#)]
93. Qi, X.; Liu, J.; Liang, Y.; Li, J.; He, S. The response mechanism of surface acoustic wave gas sensors in real time. *Jpn. J. Appl. Phys.* **2019**, *58*, 014001. [[CrossRef](#)]
94. Torad, N.L.; Ayad, M.M. Gas sensors based on conducting polymers. In *Gas Sensors*; IntechOpen: London, UK, 2019; p. 125.
95. Ma, H.; Shen, Z. Exfoliation of graphene nanosheets in aqueous media. *Ceram. Int.* **2020**, *46*, 21873–21887. [[CrossRef](#)]
96. Wei, Q.; Pei, S.; Qian, X.; Liu, H.; Liu, Z.; Zhang, W.; Zhou, T.; Zhang, Z.; Zhang, X.; Cheng, H.M. Superhigh electromagnetic interference shielding of ultrathin aligned pristine graphene nanosheets film. *Adv. Mater.* **2020**, *32*, 1907411. [[CrossRef](#)]
97. Qin, J.; Gao, J.; Shi, X.; Chang, J.; Dong, Y.; Zheng, S.; Wang, X.; Feng, L.; Wu, Z.S. Hierarchical ordered dual-mesoporous polypyrrole/graphene nanosheets as bi-functional active materials for high-performance planar integrated system of micro-supercapacitor and gas sensor. *Adv. Funct. Mater.* **2020**, *30*, 1909756. [[CrossRef](#)]
98. He, L.; Lv, H.; Ma, L.; Li, W.; Si, J.; Ikram, M.; Ullah, M.; Wu, H.; Wang, R.; Shi, K. Controllable synthesis of intercalated  $\gamma$ -Bi<sub>2</sub>MoO<sub>6</sub>/graphene nanosheet composites for high performance NO<sub>2</sub> gas sensor at room temperature. *Carbon* **2020**, *157*, 22–32. [[CrossRef](#)]
99. Yoon, H.J.; Yang, J.H.; Zhou, Z.; Yang, S.S.; Cheng, M.M.-C. Carbon dioxide gas sensor using a graphene sheet. *Sens. Actuators B Chem.* **2011**, *157*, 310–313. [[CrossRef](#)]
100. Zhu, X.; Zhou, Y.; Guo, Y.; Ren, H.; Gao, C. Nitrogen dioxide sensing based on multiple-morphology cuprous oxide mixed structures anchored on reduced graphene oxide nanosheets at room temperature. *Nanotechnology* **2019**, *30*, 455502. [[CrossRef](#)]
101. Chen, Z.; Wang, J.; Umar, A.; Wang, Y.; Li, H.; Zhou, G. Three-dimensional crumpled graphene-based nanosheets with ultrahigh NO<sub>2</sub> gas sensibility. *ACS Appl. Mater. Interfaces* **2017**, *9*, 11819–11827. [[CrossRef](#)]
102. Srivastava, S.; Pal, P.; Sharma, D.K.; Kumar, S.; Senguttuvan, T.; Gupta, B.K. Ultrasensitive Boron–Nitrogen-Codoped CVD Graphene-Derived NO<sub>2</sub> Gas Sensor. *ACS Mater. Au* **2022**, *2*, 356–366. [[CrossRef](#)]

103. Shaik, M.; Rao, V.; Gupta, M.; Murthy, K.; Jain, R. Chemiresistive gas sensor for the sensitive detection of nitrogen dioxide based on nitrogen doped graphene nanosheets. *RSC Adv.* **2016**, *6*, 1527–1534. [[CrossRef](#)]
104. Niu, F.; Shao, Z.-W.; Gao, H.; Tao, L.-M.; Ding, Y. Si-doped graphene nanosheets for NO<sub>x</sub> gas sensing. *Sens. Actuators B Chem.* **2021**, *328*, 129005. [[CrossRef](#)]
105. Singh, S.K.; Azad, P.; Akhtar, M.; Kar, K.K. High-sensitive nitrogen dioxide and ethanol gas sensor using a reduced graphene oxide-loaded double split ring resonator. *Mater. Res. Express* **2017**, *4*, 086301. [[CrossRef](#)]
106. Choi, S.-J.; Jang, B.-H.; Lee, S.-J.; Min, B.K.; Rothschild, A.; Kim, I.-D. Selective detection of acetone and hydrogen sulfide for the diagnosis of diabetes and halitosis using SnO<sub>2</sub> nanofibers functionalized with reduced graphene oxide nanosheets. *ACS Appl. Mater. Interfaces* **2014**, *6*, 2588–2597. [[CrossRef](#)] [[PubMed](#)]
107. Jiang, Z.; Li, J.; Aslan, H.; Li, Q.; Li, Y.; Chen, M.; Huang, Y.; Froning, J.P.; Otyepka, M.; Zbořil, R. A high efficiency H<sub>2</sub>S gas sensor material: Paper like Fe<sub>2</sub>O<sub>3</sub>/graphene nanosheets and structural alignment dependency of device efficiency. *J. Mater. Chem. A* **2014**, *2*, 6714–6717. [[CrossRef](#)]
108. Tanguy, N.R.; Arjmand, M.; Yan, N. Nanocomposite of nitrogen-doped graphene/polyaniline for enhanced ammonia gas detection. *Adv. Mater. Interfaces* **2019**, *6*, 1900552. [[CrossRef](#)]
109. Sett, A.; Majumder, S.; Bhattacharyya, T.K. Flexible room temperature ammonia gas sensor based on low-temperature tuning of functional groups in grapheme. *IEEE Trans. Electron Devices* **2021**, *68*, 3181–3188. [[CrossRef](#)]
110. Ahmed, M.A.; Monir, H.Q.M.; Al-Keisy, A. Evaluation of the Graphene Nanosheets as Gas Sensor for NH<sub>3</sub> Via Electrical Properties. *Surf. Rev. Lett.* **2020**, *27*, 1950215. [[CrossRef](#)]
111. Srivastava, S.; Jain, S.K.; Gupta, G.; Senguttuvan, T.; Gupta, B.K. Boron-doped few-layer graphene nanosheet gas sensor for enhanced ammonia sensing at room temperature. *RSC Adv.* **2020**, *10*, 1007–1014. [[CrossRef](#)]
112. Tian, M.; Miao, J.; Cheng, P.; Mu, H.; Tu, J.; Sun, J. Layer-by-layer nanocomposites consisting of Co<sub>3</sub>O<sub>4</sub> and reduced graphene (rGO) nanosheets for high selectivity ethanol gas sensors. *Appl. Surf. Sci.* **2019**, *479*, 601–607. [[CrossRef](#)]
113. Husain, A.; Ahmad, S.; Mohammad, F. Synthesis, characterisation and ethanol sensing application of polythiophene/graphene nanocomposite. *Mater. Chem. Phys.* **2020**, *239*, 122324. [[CrossRef](#)]
114. Fauzi, A.S.A.; Hamidah, N.L.; Kitamura, S.; Kodama, T.; Sonda, K.; Putri, G.K.; Shinkai, T.; Ahmad, M.S.; Inomata, Y.; Quitain, A.T. Electrochemical Detection of Ethanol in Air Using Graphene Oxide Nanosheets Combined with Au-WO<sub>3</sub>. *Sensors* **2022**, *22*, 3194. [[CrossRef](#)]
115. Sadasivuni, K.K.; Ponnamma, D.; Thomas, S.; Grohens, Y. Evolution from graphite to graphene elastomer composites. *Prog. Polym. Sci.* **2014**, *39*, 749–780. [[CrossRef](#)]
116. Zheng, X.T.; Ananthanarayanan, A.; Luo, K.Q.; Chen, P. Glowing graphene quantum dots and carbon dots: Properties, syntheses, and biological applications. *Small* **2015**, *11*, 1620–1636. [[CrossRef](#)]
117. Vithalani, R.; Patel, D.; Modi, C.K.; Suthar, D.H. Glowing photoluminescence in carbon-based nanodots: Current state and future perspectives. *J. Mater. Sci.* **2020**, *55*, 8769–8792. [[CrossRef](#)]
118. Kim, C.O.; Hwang, S.W.; Kim, S.; Shin, D.H.; Kang, S.S.; Kim, J.M.; Jang, C.W.; Kim, J.H.; Lee, K.W.; Choi, S.-H. High-performance graphene-quantum-dot photodetectors. *Sci. Rep.* **2014**, *4*, 5603. [[CrossRef](#)]
119. Zhang, Z.; Zhang, J.; Chen, N.; Qu, L. Graphene quantum dots: An emerging material for energy-related applications and beyond. *Energy Environ. Sci.* **2012**, *5*, 8869–8890. [[CrossRef](#)]
120. Zhu, S.; Zhang, J.; Qiao, C.; Tang, S.; Li, Y.; Yuan, W.; Li, B.; Tian, L.; Liu, F.; Hu, R. Strongly green-photoluminescent graphene quantum dots for bioimaging applications. *Chem. Commun.* **2011**, *47*, 6858–6860. [[CrossRef](#)]
121. Zhang, J.; Ma, Y.-Q.; Li, N.; Zhu, J.-L.; Zhang, T.; Zhang, W.; Liu, B. Preparation of graphene quantum dots and their application in cell imaging. *J. Nanomater.* **2016**, *2016*, 9245865. [[CrossRef](#)]
122. Sun, H.; Wu, L.; Gao, N.; Ren, J.; Qu, X. Improvement of photoluminescence of graphene quantum dots with a biocompatible photochemical reduction pathway and its bioimaging application. *ACS Appl. Mater. Interfaces* **2013**, *5*, 1174–1179. [[CrossRef](#)] [[PubMed](#)]
123. Jin, Z.; Owour, P.; Lei, S.; Ge, L. Graphene, graphene quantum dots and their applications in optoelectronics. *Curr. Opin. Colloid Interface Sci.* **2015**, *20*, 439–453. [[CrossRef](#)]
124. Chen, W.; Lv, G.; Hu, W.; Li, D.; Chen, S.; Dai, Z. Synthesis and applications of graphene quantum dots: A review. *Nanotechnol. Rev.* **2018**, *7*, 157–185. [[CrossRef](#)]
125. Shen, J.; Zhu, Y.; Chen, C.; Yang, X.; Li, C. Facile preparation and upconversion luminescence of graphene quantum dots. *Chem. Commun.* **2011**, *47*, 2580–2582. [[CrossRef](#)]
126. Zhou, C.; Jiang, W.; Via, B.K. Facile synthesis of soluble graphene quantum dots and its improved property in detecting heavy metal ions. *Colloids Surf. B Biointerfaces* **2014**, *118*, 72–76. [[CrossRef](#)]
127. Chua, C.K.; Sofer, Z.; Simek, P.; Jankovský, O.; Klimova, K.; Bakardjieva, S.; Hrdličková Kučková, S.T.P.N.; Pumera, M. Synthesis of strongly fluorescent graphene quantum dots by cage-opening buckminsterfullerene. *ACS Nano* **2015**, *9*, 2548–2555. [[CrossRef](#)]
128. Lu, Q.; Wu, C.; Liu, D.; Wang, H.; Su, W.; Li, H.; Zhang, Y.; Yao, S. A facile and simple method for synthesis of graphene oxide quantum dots from black carbon. *Green Chem.* **2017**, *19*, 900–904. [[CrossRef](#)]
129. Li, K.; Liu, W.; Ni, Y.; Li, D.; Lin, D.; Su, Z.; Wei, G. Technical synthesis and biomedical applications of graphene quantum dots. *J. Mater. Chem. B* **2017**, *5*, 4811–4826. [[CrossRef](#)]

130. Tian, R.; Zhong, S.; Wu, J.; Jiang, W.; Shen, Y.; Wang, T. Solvothermal method to prepare graphene quantum dots by hydrogen peroxide. *Opt. Mater.* **2016**, *60*, 204–208. [[CrossRef](#)]
131. Liu, B.; Xie, J.; Ma, H.; Zhang, X.; Pan, Y.; Lv, J.; Ge, H.; Ren, N.; Su, H.; Xie, X. From graphite to graphene oxide and graphene oxide quantum dots. *Small* **2017**, *13*, 1601001. [[CrossRef](#)]
132. Li, W.; Li, M.; Liu, Y.; Pan, D.; Li, Z.; Wang, L.; Wu, M. Three minute ultrarapid microwave-assisted synthesis of bright fluorescent graphene quantum dots for live cell staining and white LEDs. *ACS Appl. Nano Mater.* **2018**, *1*, 1623–1630. [[CrossRef](#)]
133. Wen, J.; Li, M.; Xiao, J.; Liu, C.; Li, Z.; Xie, Y.; Ning, P.; Cao, H.; Zhang, Y. Novel oxidative cutting graphene oxide to graphene quantum dots for electrochemical sensing application. *Mater. Today Commun.* **2016**, *8*, 127–133. [[CrossRef](#)]
134. Luo, Z.; Qi, G.; Chen, K.; Zou, M.; Yuwen, L.; Zhang, X.; Huang, W.; Wang, L. Microwave-assisted preparation of white fluorescent graphene quantum dots as a novel phosphor for enhanced white-light-emitting diodes. *Adv. Funct. Mater.* **2016**, *26*, 2739–2744. [[CrossRef](#)]
135. Zhang, X.; Wei, C.; Li, Y.; Yu, D. Shining luminescent graphene quantum dots: Synthesis, physicochemical properties, and biomedical applications. *TrAC Trends Anal. Chem.* **2019**, *116*, 109–121. [[CrossRef](#)]
136. Shinde, D.B.; Pillai, V.K. Electrochemical preparation of luminescent graphene quantum dots from multiwalled carbon nanotubes. *Chem. –A Eur. J.* **2012**, *18*, 12522–12528. [[CrossRef](#)] [[PubMed](#)]
137. Deka, M.J.; Chowdhury, D. CVD assisted hydrophobic graphene quantum dots: Fluorescence sensor for aromatic amino acids. *ChemistrySelect* **2017**, *2*, 1999–2005. [[CrossRef](#)]
138. Kang, S.H.; Mhin, S.; Han, H.; Kim, K.M.; Jones, J.L.; Ryu, J.H.; Kang, J.S.; Kim, S.H.; Shim, K.B. Ultrafast method for selective design of graphene quantum dots with highly efficient blue emission. *Sci. Rep.* **2016**, *6*, 38423. [[CrossRef](#)]
139. Russo, P.; Liang, R.; Jabari, E.; Marzbanrad, E.; Toyserkani, E.; Zhou, Y.N. Single-step synthesis of graphene quantum dots by femtosecond laser ablation of graphene oxide dispersions. *Nanoscale* **2016**, *8*, 8863–8877. [[CrossRef](#)]
140. Raeyani, D.; Shojaei, S.; Ahmadi-Kandjani, S. Optical graphene quantum dots gas sensors: Experimental study. *Mater. Res. Express* **2020**, *7*, 015608. [[CrossRef](#)]
141. Song, Z.; Huang, Z.; Liu, J.; Hu, Z.; Zhang, J.; Zhang, G.; Yi, F.; Jiang, S.; Lian, J.; Yan, J. Fully stretchable and humidity-resistant quantum dot gas sensors. *ACS Sens.* **2018**, *3*, 1048–1055. [[CrossRef](#)]
142. Jiang, W.; Chen, X.; Wang, T.; Li, B.; Zeng, M.; Yang, J.; Hu, N.; Su, Y.; Zhou, Z.; Yang, Z. Enhancing room-temperature NO<sub>2</sub> gas sensing performance based on a metal phthalocyanine/graphene quantum dot hybrid material. *RSC Adv.* **2021**, *11*, 5618–5628. [[CrossRef](#)]
143. Zhang, Y.-H.; Wang, C.-N.; Yue, L.-J.; Chen, J.-L.; Gong, F.-L.; Fang, S.-M. Nitrogen-doped graphene quantum dot decorated ultra-thin ZnO nanosheets for NO<sub>2</sub> sensing at low temperatures. *Phys. E Low-Dimens. Syst. Nanostructures* **2021**, *133*, 114807. [[CrossRef](#)]
144. Li, N.; Than, A.; Chen, J.; Xi, F.; Liu, J.; Chen, P. Graphene quantum dots based fluorescence turn-on nanoprobe for highly sensitive and selective imaging of hydrogen sulfide in living cells. *Biomater. Sci.* **2018**, *6*, 779–784. [[CrossRef](#)] [[PubMed](#)]
145. Hakimi, M.; Salehi, A.; Boroumand, F.A. Fabrication and characterization of an ammonia gas sensor based on PEDOT-PSS with N-doped graphene quantum dots dopant. *IEEE Sens. J.* **2016**, *16*, 6149–6154. [[CrossRef](#)]
146. Arunragas, S.; Seekaew, Y.; Pon-On, W.; Wongchoosuk, C. Hydroxyl edge-functionalized graphene quantum dots for gas-sensing applications. *Diam. Relat. Mater.* **2020**, *105*, 107790. [[CrossRef](#)]
147. Wongrat, E.; Nuengnit, T.; Panyathip, R.; Chanlek, N.; Hongsih, N.; Choopun, S. Highly selective room temperature ammonia sensors based on ZnO nanostructures decorated with graphene quantum dots (GQDs). *Sens. Actuators B Chem.* **2021**, *326*, 128983. [[CrossRef](#)]
148. Hong, S.-Z.; Huang, Q.-Y.; Wu, T.-M. The room temperature highly sensitive ammonia gas sensor based on polyaniline and nitrogen-doped graphene quantum dot-coated hollow indium oxide nanofiber composite. *Polymers* **2021**, *13*, 3676. [[CrossRef](#)]
149. Raeyani, D.; Shojaei, S.; Kandjani, S.A.; Wlodarski, W. Synthesizing graphene quantum dots for gas sensing applications. *Procedia Eng.* **2016**, *168*, 1312–1316. [[CrossRef](#)]
150. Chen, W.; Li, F.; Ooi, P.C.; Ye, Y.; Kim, T.W.; Guo, T. Room temperature pH-dependent ammonia gas sensors using graphene quantum dots. *Sens. Actuators B Chem.* **2016**, *222*, 763–768. [[CrossRef](#)]
151. Rahimi, K.; Yazdani, A. Ethanol-sensitive nearly aligned ZnO nanorod thin films covered by graphene quantum dots. *Mater. Lett.* **2018**, *228*, 65–67. [[CrossRef](#)]
152. Shao, S.; Chen, X.; Chen, Y.; Zhang, L.; Kim, H.W.; Kim, S.S. ZnO nanosheets modified with graphene quantum dots and SnO<sub>2</sub> quantum nanoparticles for room-temperature H<sub>2</sub>S sensing. *ACS Appl. Nano Mater.* **2020**, *3*, 5220–5230. [[CrossRef](#)]
153. Drewniak, S.; Procek, M.; Muzyka, R.; Pustelny, T. Comparison of Gas Sensing Properties of Reduced Graphene Oxide Obtained by Two Different Methods. *Sensors* **2020**, *20*, 3175. [[CrossRef](#)]
154. Zhou, Y.; Xie, G.; Xie, T.; Yuan, H.; Tai, H.; Jiang, Y.; Chen, Z. A sensitive film structure improvement of reduced graphene oxide based resistive gas sensors. *Appl. Phys. Lett.* **2014**, *105*, 033502. [[CrossRef](#)]
155. Zhou, Y.; Wang, Y.; Wang, Y.; Li, X. Humidity-Enabled Ionic Conductive Trace Carbon Dioxide Sensing of Nitrogen-Doped Ti<sub>3</sub>C<sub>2</sub>T<sub>x</sub> MXene/Polyethyleneimine Composite Films Decorated with Reduced Graphene Oxide Nanosheets. *Anal. Chem.* **2020**, *92*, 16033–16042. [[CrossRef](#)] [[PubMed](#)]

156. Hafiz, S.M.; Ritikos, R.; Whitcher, T.J.; Razib, N.M.; Bien, D.C.S.; Chanlek, N.; Nakajima, H.; Saisopa, T.; Songsirithigul, P.; Huang, N.M. A practical carbon dioxide gas sensor using room-temperature hydrogen plasma reduced graphene oxide. *Sens. Actuators B Chem.* **2014**, *193*, 692–700. [[CrossRef](#)]
157. Gupta, M.; Hawari, H.F.; Kumar, P.; Burhanudin, Z.A.; Tansu, N. Functionalized reduced graphene oxide thin films for ultrahigh CO<sub>2</sub> gas sensing performance at room temperature. *Nanomaterials* **2021**, *11*, 623. [[CrossRef](#)] [[PubMed](#)]
158. Galstyan, V.; Comini, E.; Kholmanov, I.; Faglia, G.; Sberveglieri, G. Reduced graphene oxide/ZnO nanocomposite for application in chemical gas sensors. *RSC Adv.* **2016**, *6*, 34225–34232. [[CrossRef](#)]
159. Wang, Y.; Liu, L.; Sun, F.; Li, T.; Zhang, T.; Qin, S. Humidity-insensitive NO<sub>2</sub> sensors based on SnO<sub>2</sub>/rGO composites. *Front. Chem.* **2021**, *9*, 681313. [[CrossRef](#)] [[PubMed](#)]
160. Zhang, B.; Cheng, M.; Liu, G.; Gao, Y.; Zhao, L.; Li, S.; Wang, Y.; Liu, F.; Liang, X.; Zhang, T. Room temperature NO<sub>2</sub> gas sensor based on porous Co<sub>3</sub>O<sub>4</sub> slices/reduced graphene oxide hybrid. *Sens. Actuators B Chem.* **2018**, *263*, 387–399. [[CrossRef](#)]
161. Li, Z.; Liu, Y.; Guo, D.; Guo, J.; Su, Y. Room-temperature synthesis of CuO/reduced graphene oxide nanohybrids for high-performance NO<sub>2</sub> gas sensor. *Sens. Actuators B Chem.* **2018**, *271*, 306–310. [[CrossRef](#)]
162. Song, Z.; Wei, Z.; Wang, B.; Luo, Z.; Xu, S.; Zhang, W.; Yu, H.; Li, M.; Huang, Z.; Zang, J. Sensitive room-temperature H<sub>2</sub>S gas sensors employing SnO<sub>2</sub> quantum wire/reduced graphene oxide nanocomposites. *Chem. Mater.* **2016**, *28*, 1205–1212. [[CrossRef](#)]
163. Chu, J.; Wang, X.; Wang, D.; Yang, A.; Lv, P.; Wu, Y.; Rong, M.; Gao, L. Highly selective detection of sulfur hexafluoride decomposition components H<sub>2</sub>S and SOF<sub>2</sub> employing sensors based on tin oxide modified reduced graphene oxide. *Carbon* **2018**, *135*, 95–103. [[CrossRef](#)]
164. Mirmotallebi, M.; Hosseini, Z.S.; Jokar, E. Characterization of three-dimensional reduced graphene oxide/copper oxide heterostructures for hydrogen sulfide gas sensing application. *J. Alloy. Compd.* **2018**, *740*, 1024–1031. [[CrossRef](#)]
165. Zhou, Y.; Wang, Y.; Guo, Y. Cuprous oxide nanowires/nanoparticles decorated on reduced graphene oxide nanosheets: Sensitive and selective H<sub>2</sub>S detection at low temperature. *Mater. Lett.* **2019**, *254*, 336–339. [[CrossRef](#)]
166. Jeevitha, G.; Abhinayaa, R.; Mangalaraj, D.; Ponpandian, N.; Meena, P.; Mounasamy, V.; Madanagurusamy, S. Porous reduced graphene oxide (rGO)/WO<sub>3</sub> nanocomposites for the enhanced detection of NH<sub>3</sub> at room temperature. *Nanoscale Adv.* **2019**, *1*, 1799–1811. [[CrossRef](#)]
167. Andre, R.S.; Mercante, L.A.; Facure, M.H.; Mattoso, L.H.; Correa, D.S. Enhanced and selective ammonia detection using In<sub>2</sub>O<sub>3</sub>/reduced graphene oxide hybrid nanofibers. *Appl. Surf. Sci.* **2019**, *473*, 133–140. [[CrossRef](#)]
168. Sakthivel, B.; Nammalvar, G. Selective ammonia sensor based on copper oxide/reduced graphene oxide nanocomposite. *J. Alloy. Compd.* **2019**, *788*, 422–428. [[CrossRef](#)]
169. Wang, X.; Gu, D.; Li, X.; Lin, S.; Zhao, S.; Rumyantseva, M.N.; Gaskov, A.M. Reduced graphene oxide hybridized with WS<sub>2</sub> nanoflakes based heterojunctions for selective ammonia sensors at room temperature. *Sens. Actuators B Chem.* **2019**, *282*, 290–299. [[CrossRef](#)]
170. Pasha, A.; Khasim, S.; Khan, F.A.; Dhananjaya, N. Fabrication of gas sensor device using poly (3, 4-ethylenedioxythiophene)-poly (styrenesulfonate)-doped reduced graphene oxide organic thin films for detection of ammonia gas at room temperature. *Iran. Polym. J.* **2019**, *28*, 183–192. [[CrossRef](#)]
171. Meng, F.; Chang, Y.; Qin, W.; Yuan, Z.; Zhao, J.; Zhang, J.; Han, E.; Wang, S.; Yang, M.; Shen, Y. ZnO-reduced graphene oxide composites sensitized with graphitic carbon nitride nanosheets for ethanol sensing. *ACS Appl. Nano Mater.* **2019**, *2*, 2734–2742. [[CrossRef](#)]
172. Li, Y.; Luo, N.; Sun, G.; Zhang, B.; Lin, L.; Jin, H.; Wang, Y.; Bala, H.; Cao, J.; Zhang, Z. In situ decoration of Zn<sub>2</sub>SnO<sub>4</sub> nanoparticles on reduced graphene oxide for high performance ethanol sensor. *Ceram. Int.* **2018**, *44*, 6836–6842. [[CrossRef](#)]
173. Thu, N.T.A.; Cuong, N.D.; Khieu, D.Q.; Nam, P.C.; Van Toan, N.; Hung, C.M.; Van Hieu, N. Fe<sub>2</sub>O<sub>3</sub> nanoporous network fabricated from Fe<sub>3</sub>O<sub>4</sub>/reduced graphene oxide for high-performance ethanol gas sensor. *Sens. Actuators B Chem.* **2018**, *255*, 3275–3283. [[CrossRef](#)]
174. Singh, E.; Meyyappan, M.; Nalwa, H.S. Flexible graphene-based wearable gas and chemical sensors. *ACS Appl. Mater. Interfaces* **2017**, *9*, 34544–34586. [[CrossRef](#)] [[PubMed](#)]
175. Yuan, W.; Shi, G. Graphene-based gas sensors. *J. Mater. Chem. A* **2013**, *1*, 10078–10091. [[CrossRef](#)]
176. Huang, G.; Li, Y.; Chen, C.; Yue, Z.; Zhai, W.; Li, M.; Yang, B. Hydrogen sulfide gas sensor based on titanium dioxide/amino-functionalized graphene quantum dots coated photonic crystal fiber. *J. Phys. D Appl. Phys.* **2020**, *53*, 325102. [[CrossRef](#)]
177. Smith, M.A. A Consideration of Graphite Electrodes. *IEEE Trans. Ind. Appl.* **1982**, *IA-18*, 431–434. [[CrossRef](#)]